On the manipulation of diesel particle nanostructure

Boot, Michael D.

Award date:
2005

On the Manipulation of Diesel Particle Nanostructure

Michael Boot
Reportnumber WVT 2005.13

Supervisors: ir. P.J.M. Frijters
Prof. dr. ir. R.S.G. Baert

Eindhoven University of Technology
Department of Mechanical Engineering
Division Thermo Fluids Engineering
Section Combustion Technology

Abstract

The original purpose of this study was to ascertain which chemical properties, other than fuel oxygen mass fraction, could account for the observed discrepancies in oxygenate performance reported in a previous work at this University [43]. To this end, an extensive literature research was performed on this topic. Unfortunately, the (chemical) explanations offered for the effect of oxygenates on particulate emissions, were both often limited in scope and seemingly contradictory.

It was decided then to perform yet another literature research, now focused on the (hydrocarbon) chemistry involved in particle formation. The results of this research allowed for a more in-depth investigation of the consulted literature on oxygenates. What were clearly contradictions on a macroscopic level, actually turned out to be in fact perfectly congruent from a microscopic (i.e. chemical) point of view.

Utilizing said chemical insight, it was possible to formulate a theorem that could account for and even predict oxygenate performance. As it turns out, oxygenates perform a dual task, with respect to limiting particulate emissions. One of which, namely the sequestering of carbon atoms in non-sooting species, is well established, while the second function, described here as enhancing particle reactivity, has remained hitherto in the shadows. The two, however, are unequivocally linked, considering the species thought to promote particle reactivity (i.e. C-C=O), is in fact the very molecule in which carbon is most efficiently sequestered by oxygen.

It is suggested in this work that one can enhance particle reactivity by contaminating its predominantly hexagonal (e.g. poly aromatic hydrocarbon (PAH)) nanostructure with pentagonal hydrocarbons, thereby imposing significant bond strain, which in turn causes the otherwise planar PAH to become (slightly) curved. As has been well established, the particle periphery consists primarily of concentrically tiled PAH. As particle reactivity (e.g. willingness to decompose) weighs heavily on the "tightness" with which the individual PAH are stacked, one can imagine that curved (i.e. bulky) PAH, which are inherently less tightly packed, are more prone to thermal decomposition and/or oxidation.

As it happens, the small aldehyde groups (e.g. C-C=O) mentioned earlier prove key to the formation of curvature promoting pentagonal hydrocarbons. Though more efficiently generated by fuel oxygen, said groups are likely to be formed as well in modern engines characterized by high degree of fuel / air mixing. Indeed, consulted literature on particle morphology, disclosed that a (high) degree of curvature was present in modern (i.e. Euro IV) soot particles as well.

Aldehyde groups, however, are not indispensable ingredients for the formation of curved PAH. If one were to, for example, introduce more mature (e.g. pentagonal hydrocarbons) curvature precursors to combustion chamber, one could presumably achieve a comparable degree of curvature. From this stance, it was decided to blend several molecules with Diesel fuel, which were selected solely for the resemblance they bore to the aspired pentagonal hydrocarbons.

The performance of these additives was evaluated on two heavy-duty diesel (HDD) engines and subsequently weighed against that of some established oxygenates. Though the performance of nearly all selected additives was disappointing, most likely due to a mismatch in evaporation

and/or ignition behavior, one additive (e.g. cyclohexanone) functioned exceptionally well, outperforming oxygenates as TPGME and DBM at half the fuel oxygen content (e.g. 5 vs. 9 wt-% fuel oxygen). Proving, contrary to that which is unanimously concluded in all consulted literature on oxygenates, that fuel oxygen content is not necessarily the dominant factor when it comes to the ability of an oxygenate to abate particulate emissions.

Combined with EGR and an oxidation catalyst, cyclohexanone blends were able to deliver sub-Euro V targets for all legislated emissions with only a modest decline in fuel economy, attributable, for the greater part, to the relatively low energy density of the additive in question.

Introduction

It is evident that in Europe diesel fleet emissions have a considerable impact on urban air quality. Control strategies, directed at limiting the output of these emissions, can be grouped into three distinct categories, which, in the order of upstream to downstream are: altering fuel chemistry, improving the engine design and applying aftertreatment. From both a practical and economical point of view, aftertreatment, which is designed to solve problems originating earlier in the chain, is the least attractive candidate.

Contemporary filters for trapping of particulate matter (PM) and catalysts for reducing nitrogen oxides (NO_x) may be regarded as serious bottlenecks in the engine's respiratory system, resulting in both higher fuel consumption and deteriorated engine performance. After taking into account several economical objections as well, e.g. periodical replacement (filters) and requisite precious metals (catalysts), one begins to comprehend why engine manufactures prefer to direct company resources to more upstream emission control strategies.

In the past, the engine-based emission strategies, such as raising fuel injection pressures and turbo charging were successful in lowering the yield of pollutants to their respective legislated levels. Current, and certainly future emission regulations, however, are unlikely to be met utilizing engine-based strategies alone.

Fortunately, as will be made evident throughout the course of this work, the formation rates of the most disreputable Diesel emissions, namely Oxides of Nitrogen (NO_x) and particulate matter (PM), are also a function of fuel chemistry, and from that perspective, a fuel-based emission control strategy may hold certain advantages over the more traditional engine-based approach.

The objective of this work is to study the impact of oxygenated fuels on PM emissions formed by heavy-duty diesel HDD engines on a molecular level. To this end an extensive literature research was performed, from which became evident that for a given fuel oxygen mass fraction, no credible explanation currently exists for the observed discrepancies in oxygenate performance.

In the opinion of the author, the reason that a plausible explanation has been able to remain so elusive may be traced back to insufficient emphasis on the chemistry involved in PM formation. Accordingly, this work will open with an extensive overview of the particle lifecycle on a molecular level.

Once equipped with ample knowledge on the various stages of particle evolution, the effect of fuel oxygen on PM emissions will be investigated on a molecular level as well. Emanating from said investigation is a suggested approach towards designing the optimal, with respect to abating PM emissions, fuel additive.

Finally a selection of fuel additives will be tested on two HDD engines and their performance will be subsequently weighed against that of established oxygenates such as ethanol, tripropylene glycol monomethyl ether (TPGME) and dibutyl maleate (DBM).

In order to allow the reader to become more familiar with the requisite chemical foreknowledge, the fundamentals of organic (i.e. Hydrocarbon) chemistry will be reviewed in the Appendices A thru C.

Chapter 1

Diesel Combustion Fundamentals

In order to comprehend the processes involved in the formation, growth and subsequent oxidation of particulate matter (PM), one must first become acquainted with the environment in which particle evolution takes place. To this end, a brief description of one (widely accepted) view on flame development in direct injected (DI) Diesel engines, first postulated by Dec [1] in 1997, will be reviewed throughout the course of this Chapter. Note that the conceptual model as visible in figure *1.1* has been subjected to intense investigation and has been later corroborated by, among others, Tao [2], Dahlen [3], Choi [4], and Flynn [5]. It is stressed, however, that apart from Dec in [1], no experimental confirmation of this model has been presented.

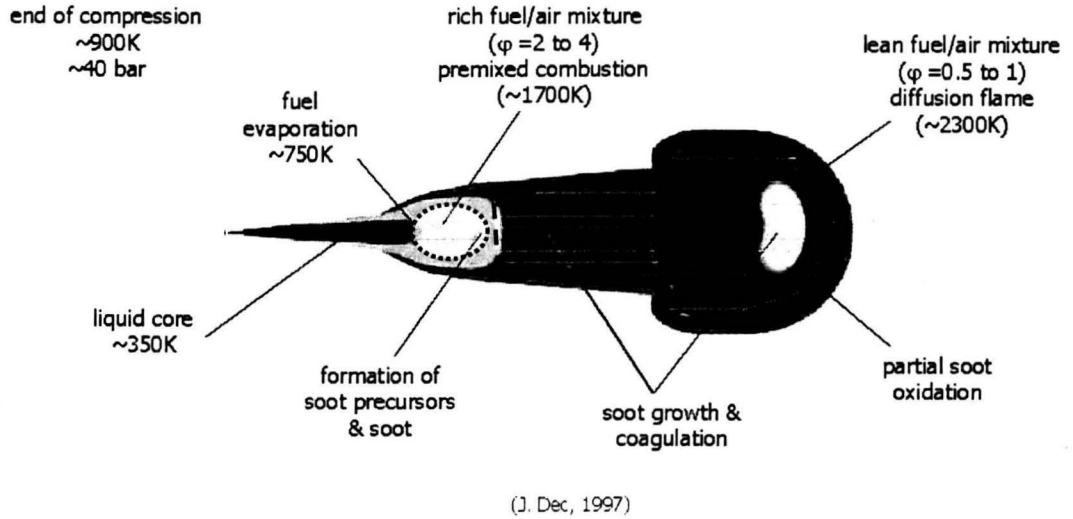

Figure 1.1: Conceptual model of flame evolution in DI Diesel engines. Adapted from [1]. The dotted area signifies the transitional zone linking evaporation and premixed combustion. The dashed area signifies the transitional zone linking premixed combustion and mixing-controlled combustion

1.1 Fuel Injection and Vaporization

Fuel injection typically commences towards the end of the compression stroke, when the prevailing in-cylinder temperature of roughly *900 [K]* is sufficiently high to rapidly vaporize the leading portion of the incoming liquid fuel jet. Throughout the vaporization process, hot air is entrained into the leading segment of the fuel jet, effectively increasing the temperature and lowering the equivalence ratio Φ.

1.2 Pyrolysis

A high temperature, oxygen deficient environment, as is the case in the fuel jet, invites a process known as pyrolysis[1]. Pyrolysis may be summarized as the thermally induced degradation of the relatively long (i.e. ~ C_{12}) fuel molecules into shorter hydrocarbons as well as a pool of methyl radicals (CH_3^-) and protons (H^+). It will be made evident in the following Chapter that CH_3^- radicals will later play a pivotal role in the formation process of PM. Protons, conversely, are critical to the oxidation process, given the fact that the principal oxidizing agents (hydroxyl (OH^-) and oxygen (O^{2-}) radicals) originate from molar oxygen having fallen prey to H^+ attack.

1.3 Auto-Ignition

In order to prompt auto-ignition, the fuel/air mixture must satisfy two cardinal prerequisites simultaneously. Primary of which is an in-cylinder temperature capable of supplying fuel molecules with sufficient thermal energy to surmount their resilience towards activation (e.g. extrication of CH_3^- and H^+). Said requisite, referred to as the auto-ignition temperature (~ 500 *[K]* for No. 2 Diesel [45]), is readily satisfied given the prevailing high temperature (~ 750 *[K]*) in the evaporation zone (figure *1.1*). Ample (i.e. $\Phi < 4$ [1]) oxygen entrainment into the fuel jet constitutes the second precondition. It is clear that these prerequisites have a complementary relationship, given the fact that a scarcity of protons will undoubtedly impair the formation of oxidation agents (e.g. OH^- and O^{2-}) regardless of the prevailing equivalence ratio.

1.4 Premixed Burn

Once ignited, the premix zone (figure *1.2*) will conduct itself as a factory converting long liquid fuel molecules into (partially oxidized) shorter chains, water, and Carbon Monoxide (CO), thereby producing trace concentrations of soot (i.e. carbonaceous core of PM) precursors as well.

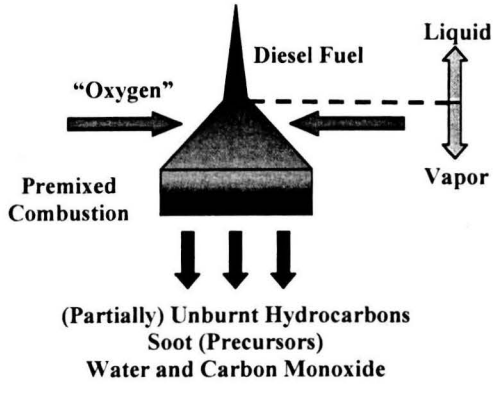

Figure 1.2: Schematic representation of premixed combustion in Diesel engines according to Dec's flame model [1]

[1] Turn to Appendix B.1 for a more comprehensive description of the chemistry involved in fuel pyrolysis and auto-ignition

1.5 Transition from Premixed to Mixing-Controlled Burn

While the remainder of liquid fuel still has to traverse the former phases, the leading pyrolysis products continue to penetrate the combustion chamber and a diffusion flame (i.e. $\Phi \sim 0.5$ to 1 and $T_{flame} \sim 2300$ *[K]*) will begin to form along the jet periphery, which will ultimately enclose the entire downstream portion of the jet [1]. Throughout the remainder of this phase, the jet will continue to grow in all dimensions and a head vortex is seen to form in the leading edge of the jet (figure *1.1*).

1.6 Mixing-Controlled Burn

Although increased in dimension, the jet pattern described above persists towards the end of injection, by which time the head vortex is well defined. In summation, it may be concluded that each fuel molecule, either leading or lagging in the jet, will undergo an analogous set of processes, i.e. injection, vaporization, pyrolysis and premixed combustion, yielding various products of incomplete combustion (figure *1.2*), which will serve as the feedstock for subsequent mixing or diffusion controlled combustion (figure *1.1* and *1.3*).

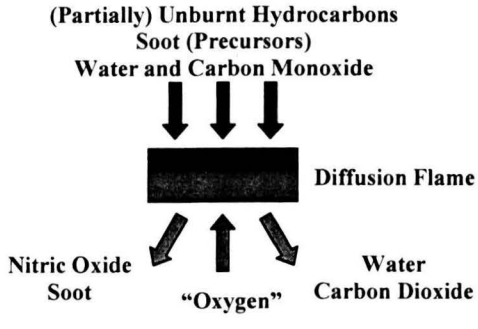

Figure 1.3: Schematic representation of mixing-controlled combustion in DI Diesel engines

Chapter 2

Lifecycle of Particulate Matter

Of all Diesel emissions, particulate matter is undoubtedly the least understood. In the past, little was known on the mechanisms involved in particle growth and oxidation. Fortunately, more recent studies [6 thru 12], utilizing Transmission Electron Microscopy (TEM), allowed the scientists involved to observe the particle nanostructure over the entire cross-section from nucleation to extinction. TEM revealed three distinct atomic configurations in Diesel soot: amorphous (i.e. disordered), graphitic (i.e. layered) and fullerene-like (i.e. curved), the subsidence of which depending primarily on pyrolytic conditions (e.g. fuel chemistry, temperature, pressure and residence time). As it turns out, many uncertainties surrounding particle evolution (figure *2.1*) can be deconvoluted when taking into account the relevance of nanostructure on particle reactivity.

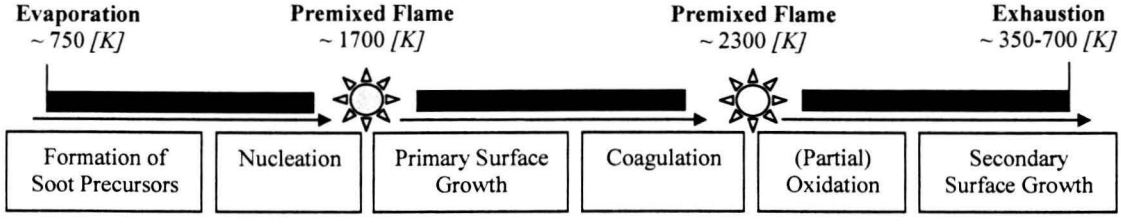

Figure 2.1: Various stages of particle evolution in DI Diesel combustion, according to the flame model of Dec [1]

2.1 Formation of Soot Precursors

Soot precursor formation is restricted to environments characterized by both high temperature and oxygen-starved conditions, alongside an ample supply of pyrolysis products. As such, soot-precursors are formed exclusively in the transitional region preceding premixed combustion (dotted area in figure *1.1*) and in the premix zone itself.

2.1.1 Mono-Aromatics

Once formed, methyl radicals can undergo a chain of reactions, which can be characterized by hydrogen abstraction and molecular growth (figure *2.2*). Nascent small, highly unsaturated species (e.g. acetylene and propargyl) can subsequently engage in auto-combination reactions to form mono-aromatics (e.g. benzene). Depicted below, are the two dominant pathways leading to Benzene.

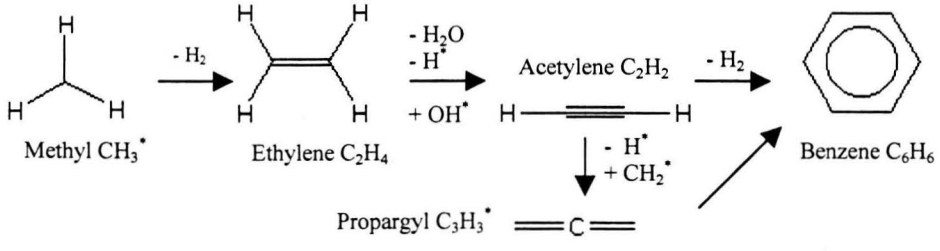

Figure 2.2: Formation of the first aromatic ring as a result of pyrolysis [13]

2.1.2 Poly-Aromatics

Potential pathways leading from the initial ring structure to poly aromatic hydrocarbons (PAH) are currently not well defined in the literature. One frequently advocated pathway, however, employs the so-called HACA mechanism (figure *2.3*).

In this mechanism, PAH growth is described as a sequential formation of higher order aromatic rings (e.g., benzene → naphthalene → phenanthrene → pyrene → higher order fused rings...), driven by **H**ydrogen **A**bstraction, activating the aromatic molecules, followed by **AC**etylene **A**ddition, promoting sustained molecular growth and subsequent cyclization.

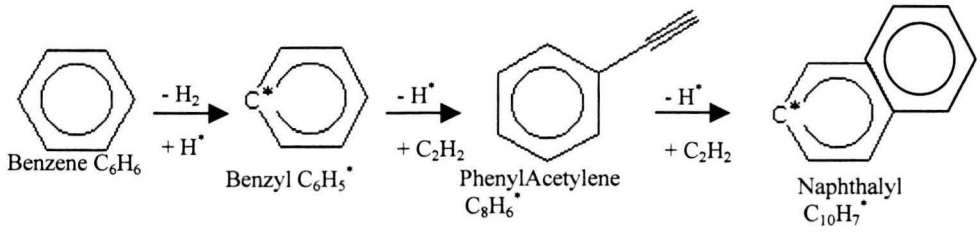

Figure 2.3: PAH growth via the HACA mechanism [14]

2.1.3 Five-Membered Impurities

Alongside the customary six-membered rings, a limited number of five-membered rings may be formed as a result of the incorporation of C2-C4 aldehydes into six-membered rings, facilitating the formation of phenoxy radicals. Subsequent decomposition of these radicals yields carbon monoxide and a cyclopentadienyl radical (figure *2.4*) [15].

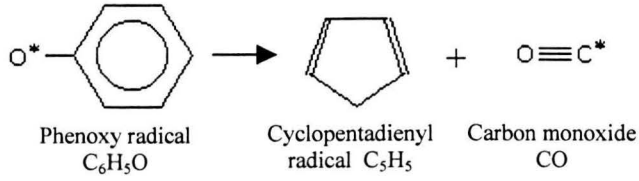

Figure 2.4: Predominant formation pathway for pentagonal impurities (e.g. Cyclopentadienyl Radicals) [15]

Assimilation, in turn, of cyclopentadienyl radicals into otherwise hexagonal PAH arrays will eventuate in tortuosity (i.e. curvature); a phenomenon illustrated below for two C_{24} isomers.

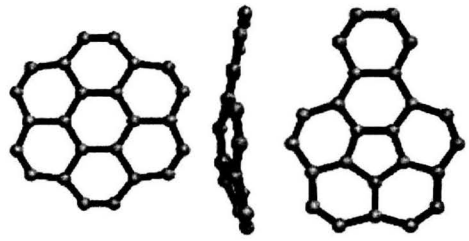

Figure 2.5: Effect of the incorporation a five-membered ring into an otherwise hexagonal array (left) [16]

It will be made evident in a later Chapter that planar and wrinkled PAH arrays each play a distinct role in the further development of soot particles. In the following paragraphs, however, the PAH arrays will be assumed perfectly flat. Tortuosity in PAH, as will be made evident later on, has a favorable effect on PM emissions.

2.1.4 Crystallites

Both PAH growth sequences will ultimately yield large two-dimensional hexagonal arrays characterized by an ever-increasing hydrogen-to-carbon ratio (HCR), owing to continuing hydrogen abstraction and acetylene addition (figure *2.7*).

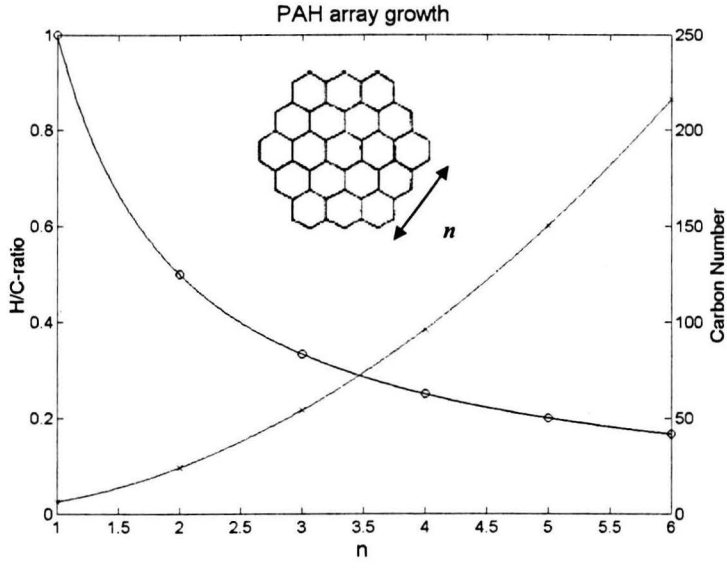

Figure 2.7: Influence of planar PAH size represented by the number of rings per side "n" on the HCR (O) and carbon number (X)

Given ample thermal energy and reaction time (paragraph 3.1.2), array growth will persist pending the attainment of a certain critical Carbon number. In this context, the critical Carbon number is defined as the minimum PAH size at which the corresponding intermolecular forces

are powerful enough to orient neighboring planes in a parallel configuration, from which point on the individual PAH involved are referred to as platelets.

The ensuing complex three-dimensional structures, commonly referred to as crystallites, are held together by relatively weak, though thermally stable Van der Waals bonds and typically consist of 2-5 platelets, with a mean layer spacing and width of *3.55 [Å]* [17] and 35 *[Å]* [8] respectively.

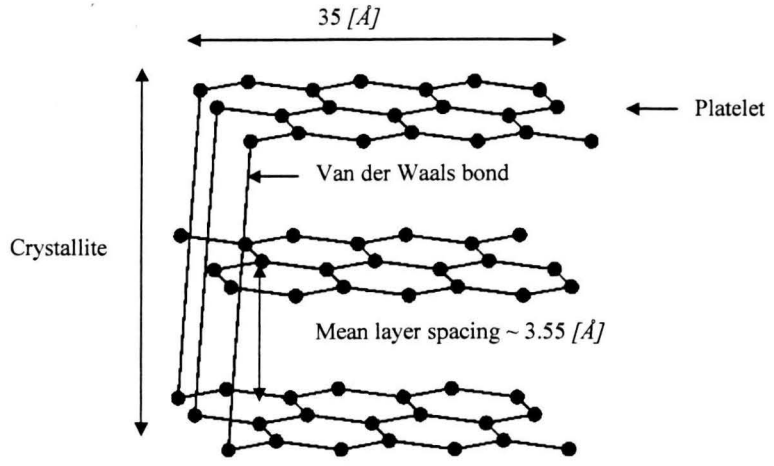

Figure 2.8: Crystallite structure held together by Van der Waals forces [18]. Note that 1 [Å] is equal to 0.1 [nm]

With estimates ranging from PAH platelets containing several tens to as many as a hundred carbon atoms, the exact value of the critical carbon number is clearly still subject of debate amongst researchers. Recent TEM observations [8] showed PAH layer planes in soot crystallites to consist of an average of 10-Benzenoids. Translating to a PAH size of $n \sim 2.25$, this observation suggest PAH platelets contain approximately 30 Carbon atoms.

2.2 Nucleation

It has been widely accepted that the visible outer surface of soot particles is made up out of crystallites, each of which comprising several platelets as illustrated in the figure below.

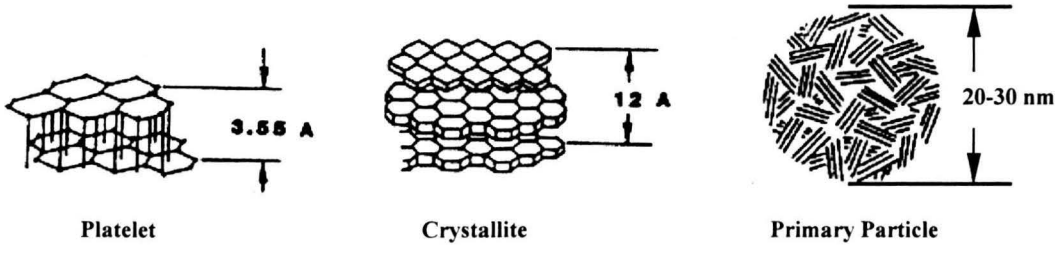

Figure 2.9: Surface structure of soot particles. Adapted from [17]

It was long thought that the structure of the particle observed at its surface was characteristic for the entire cross-section. Recent TEM observations [6, 8], however, suggests that soot particles have a more complex inner structure than previously assumed (figure *2.10*). Moreover, said radial

variation in particle nanostructure was found to be persistent regardless of operating conditions [8].

What have in the past been considered primary particles (e.g. figure *2.9*) actually contain a coagulation of even finer particles (~ 3-4 *[nm]*) that constitute their inner core. Ishiguro et al. [8] reported that, contrary to the crystalloid atomic configuration intrinsic to the particle surface, the PAH orientation in the inner particles has a more amorphous (i.e. disordered) character.

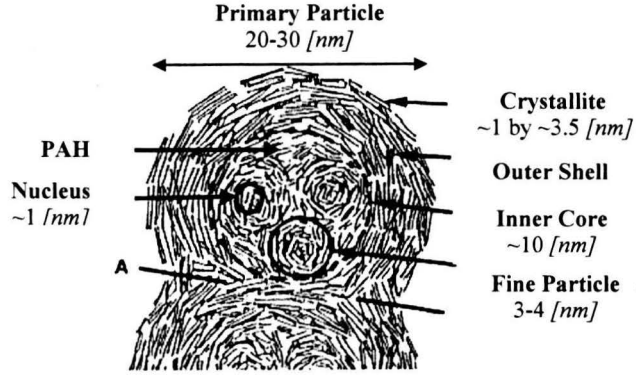

Figure 2.10: A schematic model of the nanostructure of Diesel soot based on ultra-high-resolution Transmission Electron Microscopic observations. Adapted from [8]

Attributable to collisions and the ensuing attractive dispersion forces (paragraph 2.1.4), a fraction of the gaseous PAH, discussed in paragraphs 2.1.1 and 2.1.2, will have the proclivity to cling together, ultimately forming nuclei in a process known as inception (i.e. transition from a gaseous to a solid state). The newly formed nuclei have a diameter of approximately 1 *[nm]*, corresponding to several tens of Carbon atoms. Covering the nuclei, are several Carbon layers with a turbostratic (i.e. amorphous) structure, which enlarge the nucleus diameter to 3-4 *[nm]* [8]. The nuclei are hereafter referred to as fine particles.

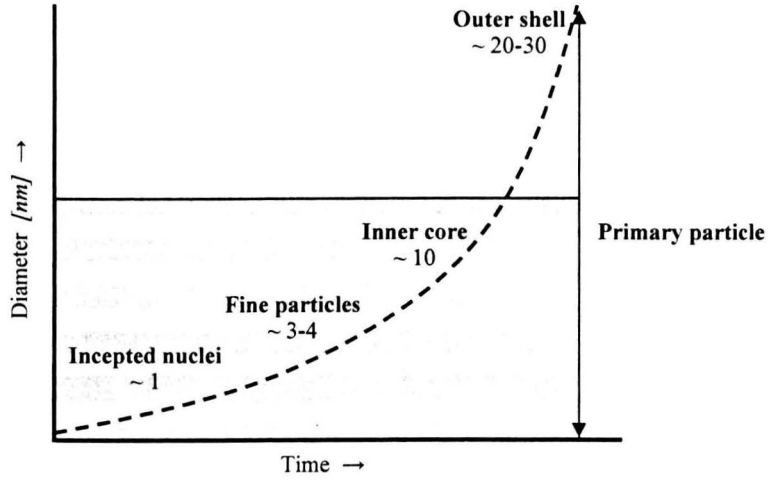

Figure 2.11: Radial evolution of primary soot particles based on the data presented in figure 2.10. The grey area encapsulates particle development prior to the premixed combustion zone

It will become clear in paragraph 2.6.3 and 3.1.1 that this turbostratic (i.e. distorted) arrangement of PAH can be attributed to the relatively low temperature environment (~ 1000-1250 *[K]*) in the transitional region preceding premixed combustion (dotted area in figure *1.1*). In this region, previously identified as the PAH formation zone, growth and subsequent crystallization of carbon lamella may be inhibited by energetics (i.e. prevailing thermal energy < activation energy) [6].

2.3 Coagulation

Following inception, inter-particle collisions will frequently force the fine particles to fuse (coagulate) into larger particles with a typical diameter of roughly 5-8 *[nm]*. As can be viewed in figure *2.10*, the coagulated particles constitute the foundation of the spheroidal inner core.

A fraction of the remaining products of pyrolysis, primarily PAH, will subsequently fill in the gaps created by the coagulated fine particles, which in turn serve as condensation nuclei, thereby forming relatively dense spheroidal cores with a mean diameter of approximately 10 *[nm]* (figure *2.10*). Note that the added segments of carbonaceous material adapt a comparable turbostratic orientation.

Said diameter, corresponding to soot collected from a black smoking Euro II/III Diesel engine [8], is roughly in line with the average diameter of shell-less amorphous soot (~ 13 *[nm]*) collected from an Euro IV engine [11, 12]. Such a striking resemblance, however, could have been predicted based on the conclusions of Vander Wal and Tomasek [6], who injected various fuels into a hot, inert (i.e. oxygen void) furnace with temperatures of 1500 *[K]* and 1900 *[K]*. They reported that, "The lower temperature yields an amorphous soot for all fuels studied here, regardless of flow rate". These results corroborate the conjectured nucleation of fine particles in the transitional zone (dotted area in figure *1.1*), which houses similar thermal conditions and, like the furnace, is characterized by the absence of oxidation.

Underwritten by several later studies [11, 12], the amorphous nanostructure of primary particle cores has been found to be omnipresent irrespective of engine technology (e.g. Euro III or IV). Dimensions and curvature of the PAH planes involved, however, were found to have a pronounced dependency on fuel chemistry (paragraph 3.2.2).

2.4 Primary Surface Growth

It may be derived, based on the literature cited above, that the amorphous particle core is formed prior to premixed combustion regardless of engine technology or fuel chemistry. Furthermore, it is assumed that the prevailing oxygen deficiency will confine oxidative attack to small C_1-C_3 species, rather than to the relatively inactive PAH that constitute the aforesaid cores (figure *2.10*).

Despite less favorable conditions, mainly owing to the presence of oxygen and further dispersion of the feedstock (e.g. gradual widening of the fuel jet), it is assumed that pyrolysis will continue to play a pivotal role in the premixed combustion zone, thus enabling supplementary PAH production. Contrary to conditions in the transitional zone (dotted area in figure *1.1*), however, the temperature increase from ~ 1000 *[K]* to ~ 1700 *[K]*, attributable to premixed combustion heat, is sufficient to surmount any thermal barriers inhibiting the realization of a more

thermodynamically favorable (e.g. graphitic) PAH arrangement (outer shell in figure *2.10*). Favorable, in this context, is defined as the minimization of both active edge sites (paragraph 2.6) and particle surface area. The former entails extended planar growth of the PAH arrays, which will persist pending the attainment of critical carbon number, as conjectured in paragraph 2.1.4.

On account of the absence of thermal barriers and the fact that the minimal surface area for any given volume is a perfectly smooth sphere, the nascent crystallites are seen to reorient themselves into concentrically tiled layers, thereby producing relatively smooth spheroidal particles with a typical diameter of 20-30 *[nm]* (figure *2.10*). On average the outer shell of primary particles contains of the order of 10^2-10^3 crystallites [17].

2.5 Agglomeration into Secondary Particles

Laser-Sheet Imaging observations performed by Dec [1] indicate that graphitic surface growth extends well into the second transitional region, which is located between the premixed- and mixing-controlled combustion zone (dashed area in figure *1.1*).

Once arrived in the turbulent head-vortex (figure *1.1*), however, a subsequent growth process, known agglomeration will gradually gain dominancy. As was the case for the preceding growth mechanisms (e.g. coagulation, condensation of PAH, primary surface growth), growth via agglomeration is driven by energetics (i.e. minimization of internal energy). Evidently, the thermal barrier of this aggregation process can be surmounted only in this oxygen deprived flame region, where turbulence driven particle collisions, combined with extreme temperatures in excess of 2000 *[K]* [1] provide the necessary activation energy. Accordingly, continued agglomeration in the oxygen-rich diffusion flame or in the relatively cool post-flame gases is not probable.

Continuously gaining stability, the individual primary particles (figure *2.10* and *2.11*) will form chain-like aggregates, hereafter referred to as secondary particles, containing tens to thousands of primary particles [17] (figure *2.12*).

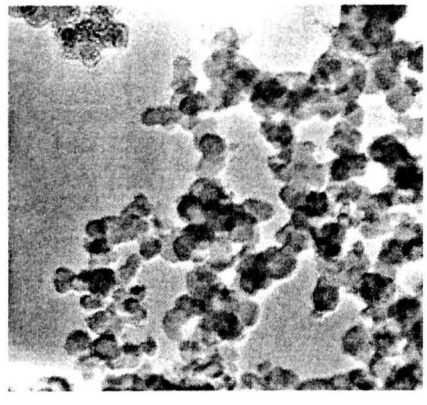

Figure 2.12: Photograph of a secondary Diesel particles, visible as an aggregate of smaller primary particles. Taken from [19]

2.6 Oxidation

As can be imagined, the mechanisms involved in particle oxidation are highly nanostructure specific. TEM measurements [7, 11] laid bare the particle oxidation process in great detail and reported dissimilar pathways for crystallite and amorphous nanostructures. Moreover, the degree of PAH curvature, induced by pentagonal impurities (paragraph 2.1.3), was reported to have a pronounced effect on particle burn rate as well. Susceptibility to oxidative attack is therefore considered both a function of plane length and orientation (i.e. crystalline/concentric vs. amorphous), as well as tortuosity.

Generally speaking, oxidative attack is confined to potentially (i.e. at typical diffusion flame conditions) active carbon sites. Activation (i.e. ionization), in this context, can transpire either via hydrogen extrication or C-C bond rupture. While the former pathway is restricted to hydrogen laden edge sites (i.e. aryl C-H bonds), the latter is restricted to susceptible basal sites (i.e. in-plane sites), weakened either by thermal or lattice defect induced bond strain.

2.6.1 Activation via Carbon-Hydrogen Bond Rupture

Activation driven by hydrogen abstraction (figure *2.13*) is the predominant pathway when hydrogen-to-carbon ratios are considered significant (i.e. ≥ 1). Although most hydrocarbons readily fulfill this prerequisite, hydrogen is quite anomalous in PAH arrays (figure *2.7*), as it is found exclusively alongside the PAH periphery.

Once activated (i.e. accommodated with free electrons), the stage is set for the ensuing chemical adsorbance of oxidative species (figure *2.13*).

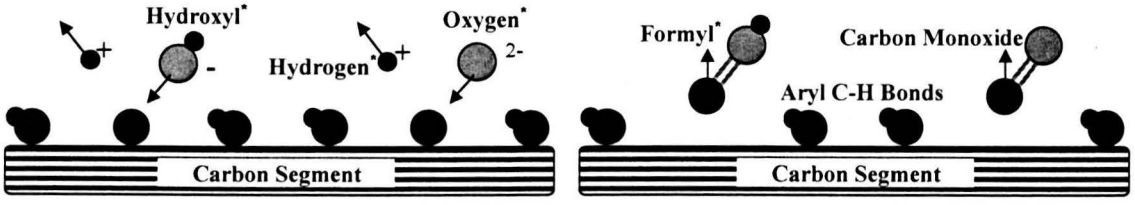

Figure 2.13 and 2.14: Activation via thermally induced Hydrogen abstraction, followed by oxidant adsorption (left). Carbon sequestration yielding oxygenated Carbon species (e.g. Formyl radicals and Carbon Monoxide) (right)

Assuming PAH reactivity is governed by the concentration of edge sites, one is able to distinguish two extremes with respect to nanostructure. Long, concentrically oriented graphitic segments, which constitute the particle shell, are practically void of edge sites, whereas the shorter, more turbostratically arranged PAH layers, intrinsic to the inner core, are characterized by a far greater concentration of carbon extremities. Moreover, the generic disordered plane arrangement of an amorphous nanostructure facilitates the accessibility of the already more abundant edge sites.

As such, oxidation initiated and sustained by hydrogen abstraction is assumed to favor an amorphous nanostructure, which is rich in edge sites, over a more compact (e.g. graphitic) one, characterized by a scarcity of said extremities.

2.6.2 Activation via Carbon-Carbon Bond Rupture

In the absence of any noteworthy tortuosity, the aforementioned aryl C-H bonds constitute the weakest (~ 413 *[kJ/mol]*) interatomic unions present in PAH arrays. As previously inferred, however, concentrations of said aryl bonds in typical Diesel soot are negligible.

Bond	**Bond Length** *[pm]*	**Bond Strength** *[kJ/mol]*
Paraffinic	154	356
Olefinic	133	636
Aromatic	139	518

Table 2.1: Bond length and strength of various classes of C-C bonds [20]

The principal interatomic bond, generic to any PAH array, is the aromatic bond. Although exceeding C-H bond strength by more than 25 % (table *2.1*), it is not inconceivable that carbon activation via aromatic bond rupture, given certain preconditions, may be a significant oxidation mechanism as well. Moreover, if aromatic bonds were to be strained by curvature, resulting from the incorporation of five-membered impurities (paragraph 2.1.3) in predominantly hexagonal arrays, the ensuing decay in electronic stability may (locally) render aromatic bonds inferior to their aryl counterparts. A recent study concerning the resilience of carbon nanotubes towards oxidation, Yang [21] reported a global attenuation in effective C-C bond strength with increasing tortuosity.

Locally, however, the destabilizing effect of lattice errors will be even more severe. As it happens, the impurities themselves (e.g. cyclopentadiene) are host to the weakest interatomic bonds.

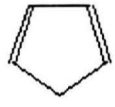

Figure 2.15: Molecular structure of Cyclopentadiene (C_5H_6)

As can be inferred from table *2.1*, these pentagonal molecules inherently contain several Paraffinic bonds, which are roughly 15 % weaker (~ 356 vs. 413 *[kJ/mol]*) than Aryl C-H bonds. Consequently, it will be these interatomic connections that are most likely to fall prey to oxidative attack.

With respect to amorphous PAH, the susceptibility towards activation will therefore increase both with the number of edge sites, as well as the relative concentration of pentagonal impurities, whereby the bonds in the latter species are most vulnerable of the two.

It is important to note that a certain level of bond strain is generic to all cyclic hydrocarbons, as their very geometry inhibits the energetically preferred tetrahedral C-C angle of 109.5°.

2.6.3 Indirect Activation

It has been made evident that the oxidation process is preceded by either C-H or C-C bond rupture. Unfortunately, the outer shell (figure *2.10*), comprising concentrically arranged crystallites, is characterized both by the absence of edge sites (e.g. aryl C-H bonds) as well as of any noteworthy tortuosity. Accordingly, it is improbable that the, otherwise undisputed, disintegration of the graphitic shell in the diffusion flame is the result of oxidants sequestering individual carbon atoms (figure *2.13* and *2.14*).

Although it is not inconceivable that thermally induced bond strain may weaken the affected aromatic bonds, thereby promoting in-plane activation via bond rupture in a manner tantamount to that discussed for lattice defect induced strain (paragraph 2.6.2), recent TEM measurements indicated a more collective breakdown, which involves entire PAH planes [9].

According to this study: "The disintegration of soot particles occurring in the late stage of oxidation is not due to the dissociation of carbon atoms at the edges of layer planes but is due rather to the stripping of small crystallites existing on the outer surface of the soot particles," and that this process "was induced by strain energy between the layer planes." The conjectured strain energy, in turn, was accredited to prior crystallite growth.

Palotas et al. [22], utilizing similar TEM technology, studied the effect of oxidation on the microstructure of carbon blacks (~ black soot), and reported a comparable crystallite growth prior to oxidation.

Tangential Growth

Ishiguro et al. [9] concluded that the prevailing temperature in or near the diffusion flame is proficient in promoting further crystallite growth in both tangential (~ 100-200 %) and radial (~ 15 %) direction, with the former preceding the latter. Growth in both dimensions was accredited to the fusion of neighboring PAH planes, rather than to thermal expansion. Since the individual planes are held firmly in place by dispersion forces (paragraph 2.1.4), tangential growth via fusion will inevitably lead to both curvature and imminent bondstrain, as is illustrated in figure *2.16*.

Said theorem is confirmed by TEM measurements that revealed the growing layer planes adopt a more "wavy shape" [9].

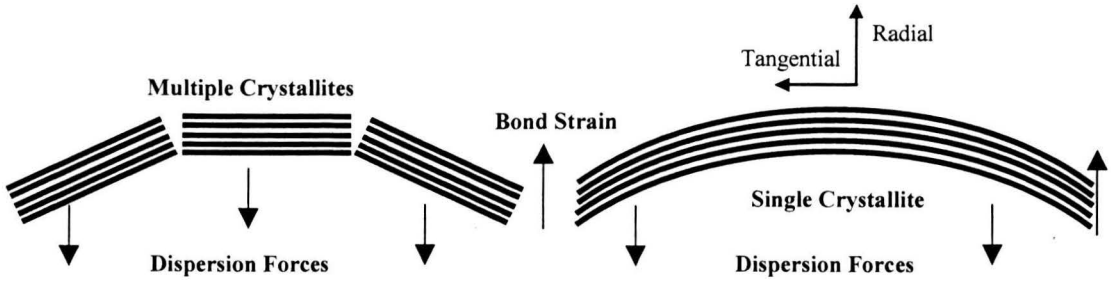

Figure 2.16: Thermally driven fusion of individual Crystallites into a single larger Crystallite

Naturally, the perturbation of PAH layers from their energetically preferred 2D planar state will provoke an electrochemical tug-of-war between curvature induced bond strain and the prevailing intermolecular forces.

Radial Growth

In response to the extended PAH surface area, the ensuing increase in dispersion force will begin to attract neighboring planes in radial direction, a phenomenon, which too, was captured utilizing TEM. Ishiguro et al. [9] reported crystallite thickness to increase from 1.4 to 1.6 *[nm]* coinciding with a reduction in interplanar distance from 0.362 to 0.355. In other words, the mean number of planes per crystallite grew from approximately 3.867 to 4.507. Palotas et al. [22] corroborated this result by reporting a monotonic decrease in inter-layer spacing with prolonged residence time in hot air (T ~ 850-950 *[K]*).

Based on the findings of Buseck et al. [23], who concluded that "the structure of amorphous cook (~ soot) becomes more orderly (i.e. crystalline) with increasing temperatures", it is feasible that disordered carbon segments, located in the particle core, may be a potential feedstock for radial crystallite growth, given their generic drive to assume the most energetically favorable orientation.

Considering the intermolecular force, which holds two bordering (i.e. in radial direction) planes together, is dictated by surface area alone, it is likely that the increase in (thickness-dependent) strain force will influence the aforementioned tug-of-war in favor of the bond strain. Ultimately, the strain force will prove victorious, manifesting in strain induced stripping of (partial) crystallites from the particle surface. Once stripped from their rigid, tightly packed arrangement, the crystallites are left with exposed edge sites, which have been previously labeled easy targets for subsequent oxidant attack.

Due to the particularly short residence time, not all soot particles will be (completely) oxidized in the thin diffusion flame. Diesel engines, however, operating at equivalence ratios under 1, are characterized by a surplus (~ 10-30 %) of oxygen in the combustion chamber. Soot oxidation will therefore persevere in the post-flame gases as long as the onset temperature window of 550-850 *[K]* for soot combustion is not breached.

Utilizing a Scanning Mobility Particle Sizer (SMPS), Lepperhoff [24] tracked in-cylinder soot levels and reported an oxidation efficiency of approximately 99% in the late combustion/early expansion phase. Although this particularly high value may not be representative for all combustion scenarios, it is reasonable to assume only a minute fraction of all the formed soot will survive the oxidation phase.

2.7 Secondary Surface Growth: Condensation

Towards the end of the expansion stroke and throughout the exhaust process, the exhaust gas temperature will have dropped to levels within the boiling range of higher-boiling UHC and eventually within that of water as well. In yet another process driven by energetics, these species have an energetically motivated tendency to condense onto secondary particles. Naturally, one

may expect heavy, high boiling species to be the first to condense, followed by lighter Hydrocarbons and finally water.

Contrary to the crystalline shell, this relatively active layer, referred to as the soluble organic fraction (SOF), can be readily disposed of in the event an oxidation catalyst is mounted in the exhaust system. Once contaminated with SOF, the secondary soot particles, as defined in paragraph 2.5, are referred to as particulate matter (PM).

2.8 Discussion

It is clear that the propensity of carbonaceous material to oxidize is highly sensitive to its nanostructure. In more explicit terms, Rosner [25] observed a 10- to 100-fold reactivity difference between the isotropic (i.e. disordered) core and graphitic shell, in favor of the former. This discrepancy was attributed to the different reactivities of carbon atoms within basal plane vs. edge site positions.

Considering both the affluence of oxygen in the diffusion flame, typically housing an equivalence ratio of 0.5 to 1, and a temperature of approximately 2300 *[K]* (figure *1.1*), it is plausible to assume the particle burn-off rate to be governed solely by nanostructure.

With nanostructure having so profound an influence on the particle oxidation rate, one might question why researchers in the field of Diesel combustion are focused on more macroscopic causality, i.e. optimization of the fuel/air mixing process (via improved fuel injection equipment (FIE), turbocharging, etc.) = less soot.

From a theoretical point of view, it might be more fruitful to actively manipulate particle nanostructure rather than to improve the (premix) equivalence ratio when ones aim is to abate engine-out PM emissions. After all, if one were able to suppress the formation of the flame-resistant crystallite shell (figure *2.10*), particulate emissions would undoubtedly drop considerably regardless of equivalence ratio.

In this, promoting the formation of lattice defects (e.g. curvature) may prove to be an effective method to inhibit individual PAH planes to form a crystalline collective. In order to ascertain how best to encourage curvature, the dependency of particle nanostructure on synthesis conditions (i.e. time, temperature, equivalence ratio, and fuel identity) should be investigated more closely.

Chapter 3

Dependence of Particle Nanostructure on Engine Operating Conditions

Chemical reaction rates involved in soot formation are governed by Arrhenian variables (i.e. temperature, concentrations of involved species (e.g. function of pressure and AFR), reaction time). It will become evident in throughout the course of this Chapter that modification of any of these variables will manifest in dissimilar nanostructure.

3.1 Physical Parameters

3.1.1 Temperature

In an Oxygen-void environment, PAH dimensions, for a given fuel identity and ample reaction time, are governed solely by energetics. As described in Paragraph 2.1.4, plane growth, crystallization and concentric reorientation are all consequences of the quest for minimum internal energy (e.g. as few edge sites as possible). In order to activate these processes, however, certain thermal barriers must be surmounted (figure *3.1*). Given the uncertainties surrounding the exact value for $C_{Critical}$ (paragraph 2.1.4) and the various thermal barriers, both the abscissa and ordinate axis are presented without an absolute scale.

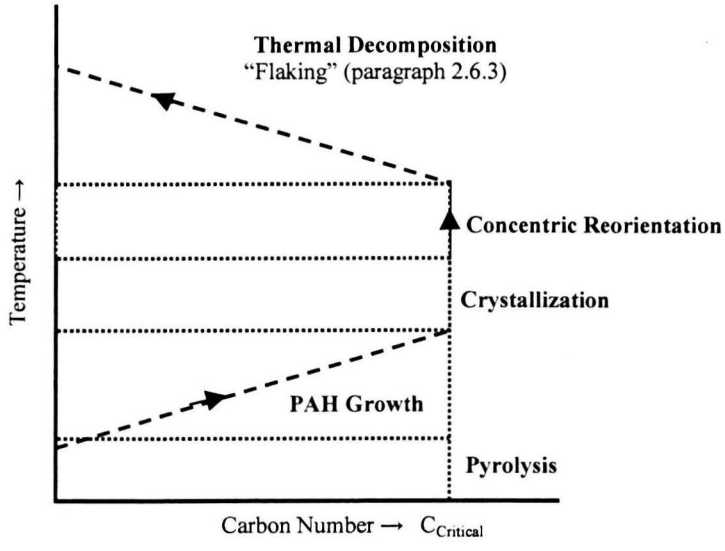

Figure 3.1: Temperature dependency of particle evolution, given an Oxygen-void environment and ample reaction time. Note that crystallization is possible only for sufficiently large PAH (Carbon number > $C_{critical}$)

The mechanism depicted in figure *3.1* is underlined by Vander Wal [6], who reported short, disordered carbon segments at low temperatures (~1500 *[K]*) and long, concentrically oriented crystallites at elevated temperatures (~1750 *[K]*), regardless of fuel composition[2]. For a given engine geometry, any augmentation in synthesis temperature is likely the result of either increased engine load and/or modified injection timing, although fuel identity and engine speed are often named as minor influences as well.

3.1.2 Residence Time

A prerequisite for an energetically (e.g. thermally) governed particle nanostructure development is ample reaction time. Although (partially) satisfied at relatively low engine speeds, the in-flame residence time of fuel molecules will typically drop with increasing engine speed. Consequently, one may expect a shift to occur from a nanostructure controlled by energetics to one being more reliant on kinetics. Soot evolution has been previously described as sequence of growth mechanisms (i.e. inception → coagulation → (graphitic) surface growth).

As radial growth is a time consuming process, the thickness of both the amorphous core and graphitic shell will reflect the residence time of the particle in the pre-premixed combustion zone (T < 750-1000 *[K]*) and post-premixed combustion zone (T > ~1750 *[K]*) respectively (figure *3.2*). Note that, as defined in Paragraph 1.5, the transitional zone implied here separates the evaporation- and premixed combustion zone (figure *1.1*).

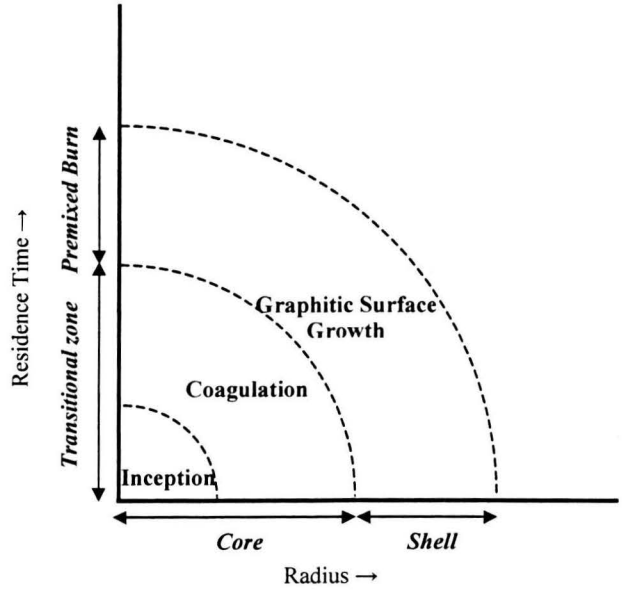

Figure 3.2: Radial particle evolution as a function of residence time in the transitional zone and premixed combustion zone

[2] Data corresponds to fuel injection into an inert furnace at relatively low flow rates (i.e. ample reaction time)

It is stressed, however, that there is one important boundary condition for the occurrence of the outer shell. Although the particle will, inescapably, spend time in both aforementioned zones, concentric tiling of crystallites will be supported only when the amorphous core has matured into a sufficiently large diameter (~ *13 [nm]* [11], ~ *10 [nm]* [8].). TEM measurements performed by Vander Wal [6] revealed shell-less soot, regardless of fuel identity or temperature, when furnace residence times where kept relatively short.

Summarizing both physical parameters, one may conclude that mean particle size augments with both an increase in load and attenuation in engine speed. In a fixed engine work point, however, combustion phasing may exert a considerable influence as well. Retarding the SOI, for example, will generally have a decelerating effect on the combustion process (i.e. less rapid premixed and more time-consuming diffusion combustion). As a result, one may assume an augmentation of in-flame residence time for soot particles and therefore a more dominant radial growth process. Note that although retarding the SOI typically lowers the (peak) flame temperature to some degree, the well-established concurrent increase in PM emissions, suggests that the thermal threshold for graphitization is surmounted nonetheless.

3.2 Chemical Parameters

3.2.1 Equivalence Ratio

For a given fuel source and synthesis temperature, the formation rate of soot precursors will be governed primarily by the average equivalence ratio in the pre-flame fuel/air jet (figure *1.1*). Said ratio, in turn, is a function of fuel/air mixing efficiency (figure *3.3*), and will tend to be more favorable (i.e. lower) for higher injection pressures and enhanced charge dynamics (e.g. swirl, tumble).

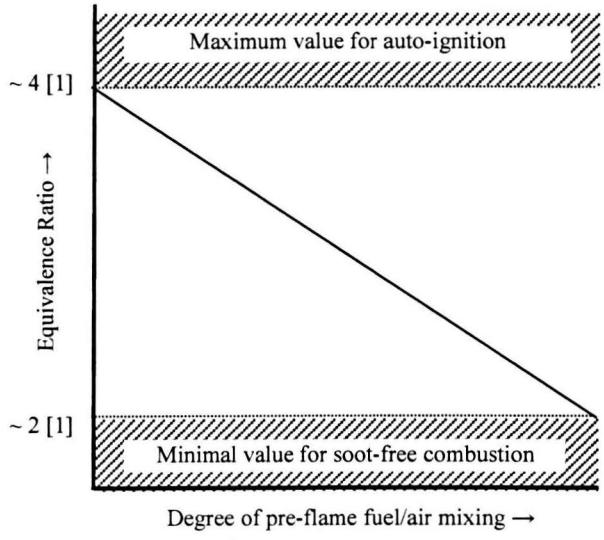

Figure 3.3: Equivalence ratio as a function of the efficiency of the pre-flame fuel/air mixing process. Note that both parameters reflect conditions in the premixed combustion zone

Equivalence ratios in premixed combustion phase are placed (by Dec [1]) between 2 and 4. A ratio in excess of 4 will not yield requisite $OH^{\cdot}$ and O^{2-} radical concentrations to warrant auto-ignition (paragraph 1.3). On the opposite end of the spectrum, premixed hydrocarbon flames with a ratio lower than 2 generally burn soot-free [26]. Gasoline engines, typically operating under stoichiometric conditions (i.e. $\varphi \sim 1$), therefore do not emit noteworthy concentrations of soot.

Apart from sequestering carbon atoms in CO, a fraction of oxygen will bond to (pyrolytically formed) C2-C4 groups thereby producing aldehydes (table *4.1*). As will be shown later on, these species, when incorporated into six-membered carbon rings, readily decompose into cyclopentadiene radicals, which in turn have proved key to promoting tortuosity in PAH arrays.

Based on this dual role of oxygen throughout the synthesis process, one would expect fewer and smaller soot particles, containing more fullerene-like graphene segments, at attenuated equivalence ratios (e.g. improved air entrainment into the fuel jet). Su et al. [12] presented TEM results that corroborate well with this theorem. The authors reported that primary particles collected from a Euro IV HDD (ETC speed B, 25 % load) had both a smaller mean diameter (i.e. ~10 vs. ~30 *[nm]*) and a more tortuous nanostructure, compared to soot collected from a black smoking Euro III HDD. While the former engine was equipped with high injection and charge pressures, the latter had been artificially adjusted to yield black soot by means of air-throttling and reduced injection pressure. Considering the altered morphology coincided with an 80 % drop in engine-out PM mass in favor of the Euro IV engine, one may infer that the number of particles must have dropped significantly as well.

3.2.2 Fuel Type

Starting from an n-paraffin, the principal constituent of Diesel fuel, the reaction pathway leading to graphitic crystallites can be summarized by the following diagram.

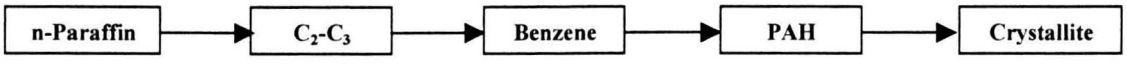

Figure 3.4: Hypothesized reaction pathway starting with n-Paraffin pyrolysis and culminating in the formation of graphitic crystallites

It is stressed here once again that, the final step in particular, requires both a high temperature (i.e. > 1700 *[K]*), as well as ample reaction time. Failure to satisfy either of these prerequisites will inhibit the formation of a graphitic outer shell (paragraph 3.1.1 and 3.1.2). Ample, as it happens, is not so absolute a concept, considering its precise value weighs heavily on both fuel type and equivalence ratio (figure *3.5*). Contemporary automotive Diesel, for example, typically contains a mono-aromatic fraction of 20-30 *[wt %]*, along with trace amounts of PAH. Effectively skipping 2-3 steps (figure *3.4*), Diesel fuels laden with a particularly high aromatic fraction (e.g. agricultural Diesel) will continue to generate black (i.e. graphitic) soot even at relatively high engine speeds and/or advanced SOI (paragraph 3.1.2).

Although the thermal threshold for crystallization is practically fixed (paragraph 3.1.1), the required residence time for crystallite/graphitic shell formation is assumed to shift as a function of fuel composition.

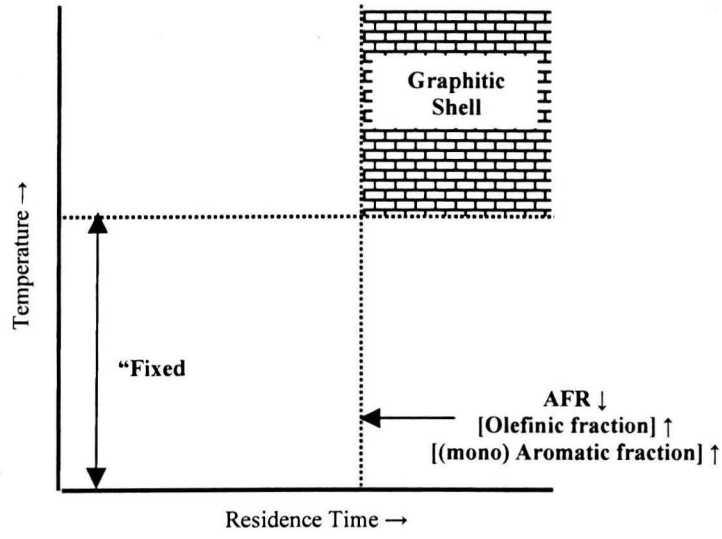

Figure 3.5: Influence of equivalence ratio and fuel identity on the time required to form a graphitic outer shell. Note that the requisite reaction time attenuates as the fuel contains more soot-precursors (Unsaturated/Aromatic Carbon bonds]

At a given synthesis temperature, the rate at which PAH obtain critical (i.e. warranting crystallization) dimensions is governed by the concentrations of primary (C_2-C_3) and secondary (C_6H_6) PAH feedstocks (figure *3.5*). While the latter can be introduced directly via the fuel, the prevalence of the former species is extremely sensitive to both the equivalence ratio as well as the predominant hydrocarbon class present in the fuel. Accordingly, high oxygen concentrations readily translate into a higher degree of carbon sequestration (i.e. CO production), and therefore fewer C_2-C_3 precursors. Pertaining to fuel identity, the efficacy of carbon sequestration augments with the level of saturation. In other words, neighboring carbon atoms sharing a double bond (e.g. olefins) will tend to remain interconnected, thereby increasing the yield of C_2 species in particular.

As argued earlier, curvature is a consequence of the incorporation of pentagonal impurities into the predominantly hexagonal PAH arrays. For given synthesis conditions, it is therefore plausible to assume the degree of curvature to be proportionate to the yield of cyclopentadiene. Having C_2-C_3 aldehydes as primary building blocks (paragraph 5.1), it is assumed that the ability of a fuel to generate said impurities will ultimately determine the level of tortuosity.

Stable molecules such as (mono-) aromatics will tend to decompose at higher onset temperatures than the more reactive paraffins. As a result, the former hydrocarbon class will generally yield fewer C_2-C_3 species, requisite to PAH curvature, than the latter.

This theorem is in agreement with findings presented by Vander Wal [6], who reported a higher degree of tortuous nanostructure in the order pyrene ($C_{16}H_{10}$) → naphthalene ($C_{10}H_8$) → benzene (C_6H_6) → acetylene (C_2H_2).

3.3 Discussion

As concluded in the previous Chapter, promoting PAH curvature may very well prove to be the most effective method to reduce engine-out PM emissions. Tortuous PAH hold two intrinsic advantages over their planar counterparts, the most obvious of which, extensively discussed in the foregoing paragraphs, is related to their relative weak mean C-C bond strength. Induced both by the curvature itself (e.g. bondstrain) as well as the presence of inherently weak paraffinic bonds located in the pentagonal impurities (figure *2.15*), the attenuation in bondstrength renders curved PAH more susceptible to oxidative attack.

Although less evident, but nonetheless of great significance, is the resilience of curved PAH to stack within inter planar distances requisite for dispersion forces to become of significance (~ 30-40 *[nm]*, paragraph 2.1.4). Indeed, no literature account of a graphitic shell was found when the core consisted of fullerene-like carbon segments. Apparently, intermolecular forces in a typical Diesel flame environment do not surmount the energy required to "squish" curved PAH into a crystalline geometry.

The yield of curvature inducing precursors (i.e. C_2-C_3 aldehydes) is controlled both by the propensity of fuel molecules to (pyrolytically) break-off C_2-C_3 species and the local equivalence ratio in the synthesis zone. Over the years, fuel and engine modifications have led to a more favorable (i.e. unfavorable for PAH formation) synthesis environment. Consequently, the dominant particle nanostructure has gradually shifted from a rather rigid core-shell configuration to one uniquely comprising curved PAH.

The achieved reduction in PM emissions from 0.36 (1992:Euro I) to 0.10 *[g/kWh]* (2000: Euro III) is commonly attributed to lowered concentrations of soot precursors (i.e. Acetylene / Benzene) and growth species (i.e. Sulphates/UHC). Altered particle nanostructure (e.g. curved vs. graphitic), which manifests in significant higher PM burn-rates, is scarcely named as a prospective contributor to the realized reduction in PM concentrations.

Today's Diesel fuel, practically void of any Sulphur or Aromatics, leaves little room for "traditional" fuel improvements. Moreover, with current injection pressures, in excess of 2000 *[bar]*, already pushing the technical envelope, a subsequent doubling does not seem not probable from a practical point of view. The fact that the automotive industry is relying heavily on aftertreatment, rather than on engine modifications, to meet their 2005 target (i.e. Euro IV: 0.02 *[g/kWh]*) is a testimonial to the aforementioned technical limitations.

As will be elaborated on more extensively in the following Chapter, oxygenated fuels, such as ethanol, contain one or more oxygen atoms in their molecular structure. Depending on the location and type (i.e. single or double bond) of carbon-oxygen bonds involved, oxygenates may facilitate direct extrication of aldehydes (figure *3.6*).

Ethanol C_2H_5OH Acetaldehyde C_2H_4O Hydrogen H_2

Figure 3.6: Predominant decomposition pathway of Ethanol

Reactions involving both oxygenated (e.g. Aldehydes) and non-oxygenated C_2-C_3 species frequently eventuate in the formation of Phenoxy radicals (figure *3.7* and *3.8*).

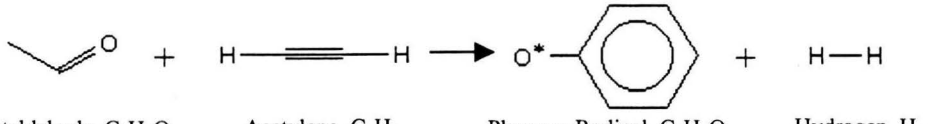

Acetaldehyde C_2H_4O Acetylene C_2H_2 Phenoxy Radical C_6H_5O Hydrogen H_2

Figure 3.7: Phenoxy Radical formation via combination of oxygenated and non-oxygenated C_2 molecules

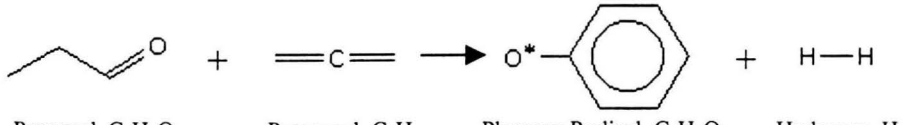

Propanal C_3H_6O Propargyl C_3H_4 Phenoxy Radical C_6H_5O Hydrogen H_2

Figure 3.8: Phenoxy Radical formation via combination of oxygenated and non-oxygenated C_3 molecules

Accordingly, many Oxygen-laden fuels are capable of generating Phenoxy radicals in a more direct fashion, often yielding a highly curved nanostructure regardless of equivalence ratio or residence time.

Vander Wal [6] reported that "Ethanol uniquely yielded a soot with a high degree of curvature", regardless of residence time. Translated into engine jargon this entails that, when fuelled with ethanol, parameters that govern in-flame residence time (e.g. engine speed and combustion phasing (paragraph 3.1.2)) may be chosen at will without the risk of forging nearly incombustible graphitic particle shells (figure *2.10*).

Chapter 4

Impact of Fuel Oxygen on Particle Evolution

4.1 Oxygenates: A Brief Literature Review

Adding oxygenates to regular Diesel fuel has been frequently proposed as a promising technique to reduce engine-out PM levels. The consulted literature on this topic [27, 28, 30-36, 38-43 and 46-61] consistently reported a significant reduction in PM emissions when oxygenates were blended with the base fuel. In the majority of studies [28, 31, 34, 40, 43, 46-48, 50, 52-54, 56, 57 and 61], said decrease was found to be nearly proportionate to the mass fraction of oxygen in the fuel. Moreover, some authors reported soot-free combustion (in DI Diesel engine) when the mass fraction of fuel oxygen is in the range 25-40 wt-% [27-30 and 61].

Reference	Blended Oxygenate	Fuel Oxygen Content required for Soot-free Combustion
Cheng [27]	Dimethoxy methane: $C_3H_8O_2$ Ethanol: C_2H_6O	30-40 wt-%
Curran [28]	Methanol: CH_4O Ethanol: C_2H_6O	35-42 wt-%
Flynn [29]	Methanol: CH_4O	25-30 wt-%
Miyamoto [30]	Diethylene glycol dimethyl ether: $C_6H_{14}O_3$ Ethylene glycol mono-n-butyl ether: $C_6H_{14}O_2$	27-36 wt-%
Musculus [61]	Various paraffinic oxygenates	~30 wt-%

Table 4.1: Accounts of soot free burning Diesel/Oxygenate blends found in literature

The beneficial impact of fuel oxygen on particulate emissions is frequently accredited to enhanced 'trapping' of carbon in non-sooting species (e.g. partially oxidized C_1-C_2 hydrocarbons) [27, 28, 35, 38, 40, 48, 52, 55, 59 and 60]. In other words, by means of bonding oxygen directly to carbon, fewer carbon atoms are available to mature into (potential) soot precursors (e.g. ethylene, acetylene, etc (paragraph 2.1). At a fixed fuel-oxygen level, however, carbon sequestration was often found to be dependent on the functional oxygen groups (table *4.2*) involved [27, 31, 36 38-40 and 47-49].

Chemical Class	Functional Oxygen Group	Formula
Alcohol	*Hydroxyl*	R-OH
Carbonate	*Carbonate*	R_1-O-C (=O)-O-R_2
Carbonyl	*Aldehyde*	R_1-C (=O)-H
	Ketone	R_1-C (=O)-R_2
Carboxylic Acid	*Carboxyl*	R_1-C (=O)-OH
Ether	*Ether*	R_1-O-R_2
Ester	*Ester*	R_1-C (=O)-O-R_2

Table 4.2: List of functional oxygen groups with their respective formulae

In some studies, other blend properties including cetane number [40] and boiling behavior [34,38] were named as (possible) contributors to the observed discrepancy in oxygenate as well. A consistent explanation as to why one oxygenate outperforms another at a fixed fuel oxygen percentage, however, could not be found in the examined literature.

It is probable, however, as will be made evident in the following paragraph, that improved carbon sequestration is not the only mechanism via which fuel oxygen can reduce PM emissions. A second, hitherto overlooked mechanism, is rooted in the fact that C_2-C_3 aldehydes, previously identified as probable precursors of curved PAH, are formed directly as a result of oxygenate pyrolysis. With non-oxygenated fuels, said species can only be formed later on in the premixed zone (figure *1.1*). Accordingly, fuel oxygen may (indirectly) facilitate the formation of curvature precursors at an earlier time in the particle evolution (Chapter 2).

4.2 Fuel Oxygen as a Means to Promote a Curved Particle Nanostructure

In addition to serving as an excellent sequestering agent for fuel carbon (paragraph 4.1), C_1-C_2 aldehydes may play a more obscure role in the manipulation of particle evolution. Previously argued in paragraph 2.1.3, a chemical reaction involving both acetaldehyde as well as acetylene will generally lead to the formation of Phenoxy radicals (figure *4.1*).

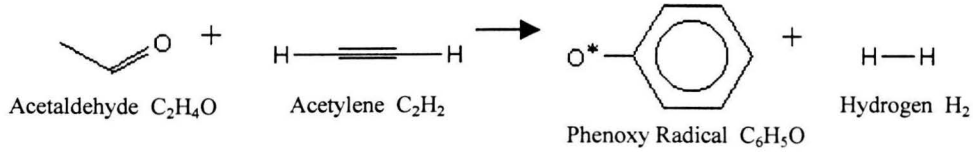

Figure 4.1: Phenoxy Radical formation via combination of oxygenated and non-oxygenated C_2 molecules

Subsequent decomposition of said species tends to generate cyclopentadienyl radicals (figure *4.2*) along with carbon monoxide; the former of which is believed to play a pivotal role in the formation of curved PAH (paragraph 2.1.3). VanderWal [6] observed the pyrolysis process of ethanol utilizing TEM and reported this alcohol to yield "a highly curved particle nanostructure".

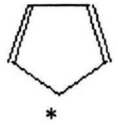

Figure 4.2: Cyclopentadienyl radical (C_5H_5)

Consequently, one may expect the degree of tortuosity to augment with the concentration of acetaldehyde. In other words, the particle nanostructure may shift from graphitic to fullerene-like (figure *2.5*) with increasing fuel oxygen content. Regrettably, documentation on the effect of oxygenated fuel on particle nanostructure is at the present rather limited.

4.3 Drawbacks of Oxygenated Fuels

A well-known ailment of oxygenated fuels in general is their tendency to increase engine-out Aldehyde emissions [35]. Although currently not subjected to (automotive) legislation, aldehydes have several malevolent effects on human health (e.g. Carcinogeous, irritant to the respiratory system) and the environment (e.g. smog). It is therefore conceivable that a widespread introduction of oxygenated fuels may invite stringent aldehyde legislation. Considering NO_x emissions are often invariable to fuel oxygen content, the utilization of oxygenated fuel will most likely replace the current NO_x/PM-tradeoff with an aldehyde/PM tradeoff.

Taking into account the high fuel oxygen content (i.e. ~30-40 wt-%) required to abate PM emissions to negligible levels (table *4.1*), implementation of this approach would imply fuelling engines with, by approximation, neat oxygenates. Apart from having a characteristically low heating value, neat oxygenates will undoubtedly be more costly than contemporary Diesel. From an economical point of view, light alcohols (e.g. ethanol), which can be synthesized from a biological feedstock, are currently the only viable oxygenates. Unfortunately, the detrimental ignition behavior (i.e. CN ~ 8 vs. ~ 50 for Diesel), generic to all polar molecules, will necessitate the addition of a significant concentration of ignition improver. Furthermore, given the relatively low boiling point (e.g. ~350 *[K]*) of ethanol, additional measures will have to be undertaken to inhibit the formation of vapor bubbles in the FIE system.

4.4 Discussion

One may summarize that, with respect suppressing PM emissions, fuel oxygen is likely to play a double role:

1. (Partially) inhibits the formation of soot precursors via sequestration of fuel carbon into non-sooting species
2. Promotes the formation of tortuous PAH via formation of C_2-C_3 aldehydes as a result of oxygenate pyrolysis

It is interesting to note that both *1* and *2* have been observed (e.g. TEM measurements) as well in modern engines (e.g. Euro IV HDD) running on non-oxygenated fuel [11, 12]. The apparent irrelevance of the origin (i.e. oxygenate or improved fuel/air mixing) of the supplementary oxygen in the synthesis zone is in agreement with an earlier study performed by Donahue and Foster [60]. Donahue and Foster concluded that "oxygen enhancement, whether it be from intake air enrichment or via oxygenated fuels, reduces particulate matter", with the effectiveness "depending on the local concentration of oxygen in the fuel plume". For now, it remains uncertain which of the two (e.g. enhanced fuel/air mixing vs. fuel oxygen) is the more effective approach to lower PM emissions.

What is certain, however, is that the greater majority (e.g. up to 99 % [24]) of the formed soot particles will fall prey to oxidation in the late combustion/ early expansion phase, regardless of engine technology or fuel oxygen content. Even in the event this value is slightly exaggerated, it still implies that most soot precursors will not mature into engine-out PM, and can therefore be considered relatively harmless.

Granted that both more advanced FIE and combustion chamber geometry, as well as fuel oxygen, hold the promise to attenuate PM concentrations to negligible levels, it is debatable, given the above theorem, if raising oxygen levels in the synthesis zone is the most cost-effective way to exterminate the relatively scant amount of particles that survive the oxidation phase.

In the view of the author it may therefore be more fruitful to lay more emphasis on enhancing particle burn rate rather than on reducing its feedstock. In this, promotion of curved PAH might prove to be key. It has been reported in the literature that a shift from graphitic to fullerene-like nanostructure will coincide with a substantial (e.g. x 4 [7], x 5 [8]) increase in particle burn-rate.

Chapter 5

Search for Curvature Promoting Fuel Additives

Starting from Diesel fuel, the pathway leading towards curved PAH involves the formation and consumption of several intermediate species, as is illustrated in the figure below.

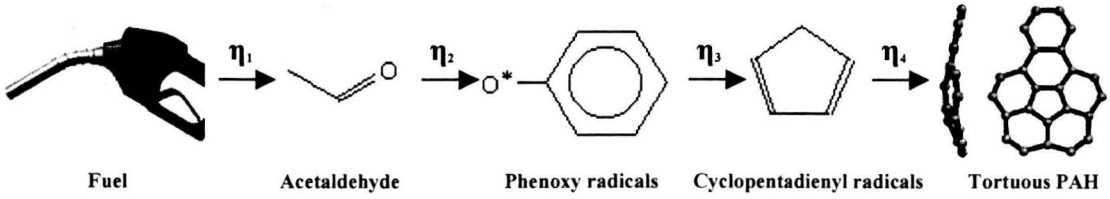

Figure 5.1: From fuel to tortuous PAH

5.1 Acetaldehyde

Each step in said sequence has a certain, at this time unknown, conversion efficiency. It is assumed here, given the higher concentrations of oxygen in the synthesis zone (Chapter 4), that contemporary measures aimed at abating engine-out PM emissions have, albeit inadvertently, already led to an increased in η_1 (figure *5.1*). Concentrations of subsequent intermediate species have undoubtedly profited from this augmentation, given the observed shift from the (traditional) graphitic to more fullerene-like particle nanostructures, the latter of which having been detected in exhaust streams of modern (i.e. Euro IV) engines [11, 12].

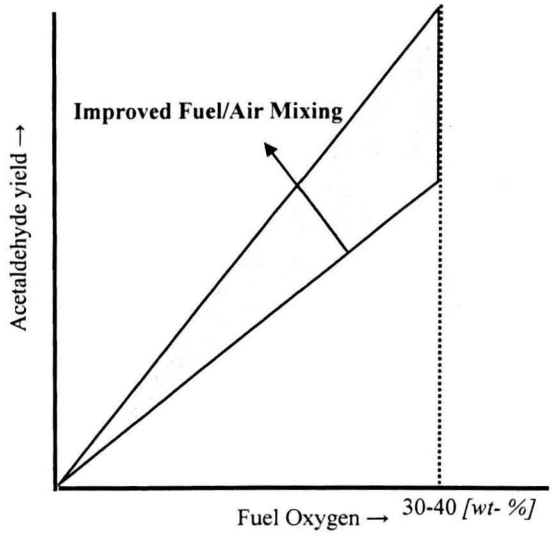

Figure 5.2: Qualitative prediction of the acetaldehyde yield in the particle synthesis zone (Chapter 2) as a function of fuel/air mixing and fuel oxygen content

In the view of the author, the ultimate objective of fuel modification should be the promotion of PAH tortuosity. Ergo, one may assume that doping Diesel fuel with certain molecules, designed specifically to mimic (i.e. with respect to structure) curvature precursors (figure *5.1*), will yield a more tortuous particle nanostructure than achieved otherwise via oxygen enrichment of the particle synthesis zone (e.g. oxygenates and/or enhanced fuel/air mixing).

5.2 Phenoxy Radicals

5.2.1 Phenol

As can be gathered from figure *5.1*, the formation of acetaldehyde via fuel pyrolysis is merely the first step of many leading to the aspired tortuous nanostructure. It is assumed that the second step in particular is fairly rare, considering the rather remote probability of an acetaldehyde molecule colliding with as many as two C_2-molecules (e.g. acetylene) (figure *5.3*).

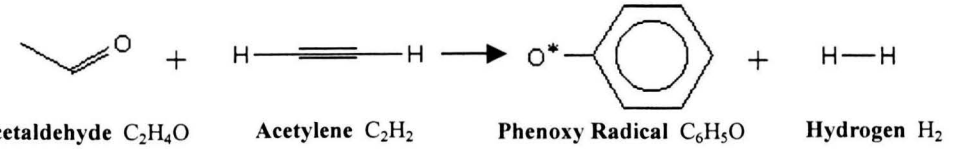

Figure 5.3: Phenoxy Radical formation via combination of oxygenated and non-oxygenated C_2 molecules (see also figure 3.7, p. 23)

Consequently, one may expect the concentration of phenoxy radicals to be relatively low compared to that of acetaldehyde. The question at hand is therefore how best to amplify the number of phenoxy radicals in the particle synthesis zone. An obvious choice would be to introduce phenoxy radicals directly into the combustion chamber via the fuel. Unfortunately, as this species, like all radicals, is highly unstable, a phenoxy radical will have to be contained within a more stable molecule, the most obvious host being phenol.

Figure 5.4: Molecular structure of phenol. Note that the grey, white and red atoms represent carbon, hydrogen and oxygen respectively

Regrettably, the presence of a polar (e.g. OH^-) group on the benzene ring elevates the melting point to an unacceptable high level (e.g. 315 *[K]*). More complicated variants containing one or more alkyl-groups have slightly lower melting points, though still unacceptable nonetheless. In addition to unfavorable melting behavior, the skeletal constituent of phenol, benzene, is an infamous carcinogen.

5.2.2 Cyclohexanone

A non-aliphatic molecule, which closely resembles phenoxy radicals, is cyclohexanone (figure *5.5*). This molecule, now held together by paraffinic rather than the aforementioned aromatic bonds, not only has far less detrimental anthropological properties, but a substantially lower (i.e. more desirable) melting point as well (i.e. ~ 225 *[K]* vs. ~ 315 *[K]*).

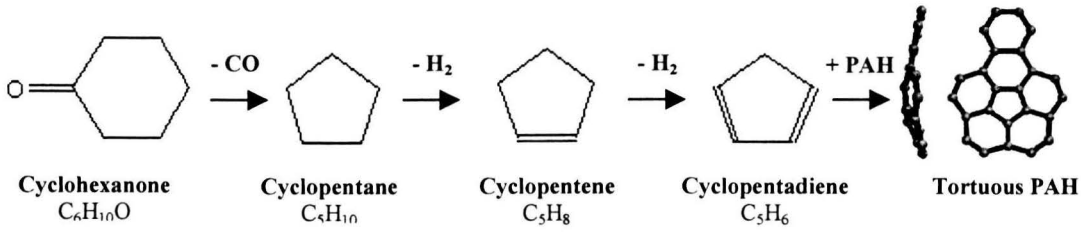

Figure 5.5: Assumed reaction pathway to tortuous PAH via cyclohexanone

Considering the common characteristics of cyclohexanone and phenoxy radicals with respect to molecular structure, it is assumed here that the decomposition pathways will bare a similar congruity. The absence of requisite unsaturated bonds, however, necessitates subsequent hydrogen abstraction and olefinization, although said reactions typically thrive in the high temperature, oxygen-poor synthesis zone (paragraph 1.2 and 1.3).

5.2.3 Cyclohexane

In addition to carbon extrication via oxygenation (e.g. cyclohexanone), the aforementioned conditions in the synthesis zone may promote conversion of C_6 to C_5-molecules via methylene (CH_2^*) scission as well (figure *5.6*). Accordingly, non-oxygenated hexagonal hydrocarbons such as cyclohexane, could culminate in tortuous PAH via the reaction pathway given below:

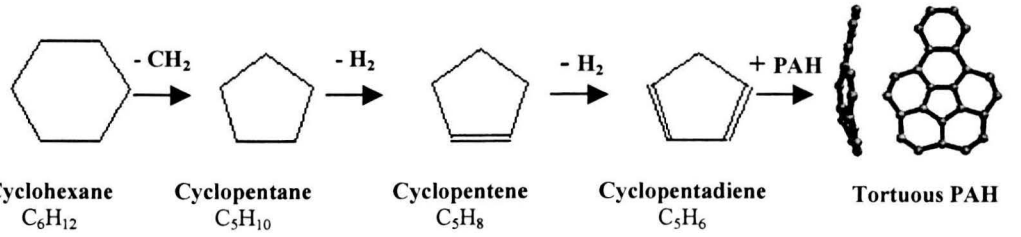

Figure 5.6: Assumed reaction pathway to tortuous PAH via Cyclohexane

From a practical point of view, one would prefer cyclohexane to cyclohexanone, both in terms of heating value (~ 41 vs. 31.4 *[MJ/kg]*) and availability. Cyclohexane can be readily derived from (mono) aromatics, a natural component in contemporary Diesel fuel (e.g. 20-25 wt% in U.S. NO. 2), via an elementary hydrogenation process (figure *5.7*).

Attainment of cyclohexanone would require two additional steps, namely hydrogen abstraction and oxygen addition (figure *5.7*).

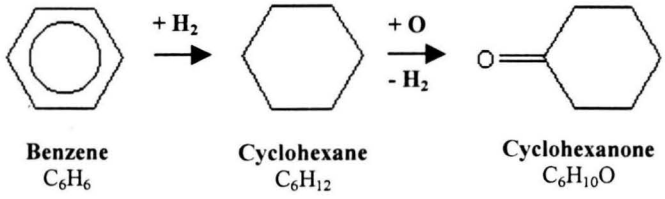

Figure 5.7: Procurement of Cyclohexane and Cyclohexanone from a mono-Aromatic feedstock

5.3 Cyclopentadiene Radicals

Instead of hexagonal additives, one could off course consider to dope Diesel directly with pentagonal hydrocarbons. With respect to curvature promotion, one would naturally expect said molecules (e.g. cyclopentane) to perform better, bearing in mind the end product allows for the carbon chain to remain in tact (figure *5.7*).

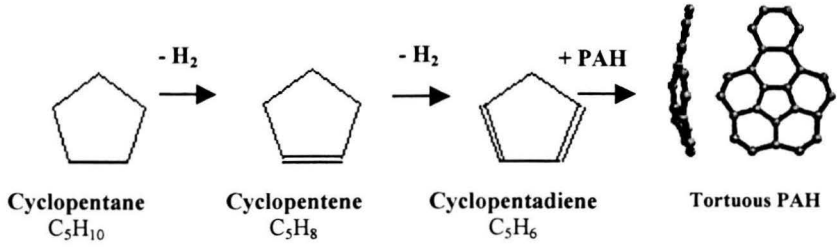

Figure 5.7: Assumed reaction pathway to tortuous PAH via Cyclopentane

Pentane, however, given its relatively high volatility (i.e. $T_b \sim 309$ *[K]*) may invite vapor bubbles throughout its passage in the FIE system (see also light alcohols, paragraph 4.2.3). As was the case for the conversion rate of cyclic C_6 molecules to C_5 species, no estimation is currently available for the degradation rate of C_5 naphthenes to useless C_4 species.

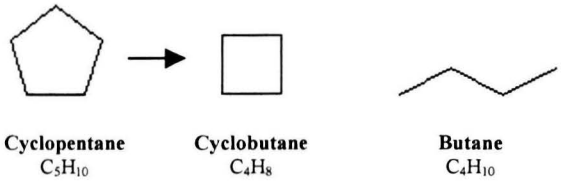

Figure 5.8: Degradation of Cyclopentane to C_4 chains

5.4 Tortuous PAH

Ideally, one would prefer to introduce tortuous PAH directly into the combustion chamber. Unfortunately, melting points well above room temperature, intrinsic to such heavy aromatic molecules, are sufficient grounds to discard them as potential Diesel additives. Perhaps second to best is a tortuous mono aromatic hydrocarbon known as indene.

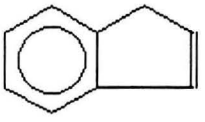

Figure 5.9: Molecular structure of Indene (C_9H_8)

Indene, harboring both a hexagonal and pentagonal component is present by definition in curved PAH, as is pictorially illustrated in the figure below.

Figure 5.10: Location of an Indene-like molecule (e.g. dashed red line) within tortuous PAH. Adapted from [16]

5.5 Discussion

Presented below (table *5.1*) is an overview of the thermodynamic properties of the additives chosen for this study, as well as their respective positions within assumed curved PAH reaction mechanism. Based purely from a chemical viewpoint, one may surmise that additive performance will improve, as the molecule in question resembles more mature curvature precursors. As such, cyclopentane, and Indene in particular, should outperform their hexagonal counterparts, cyclohexanone and cyclohexane.

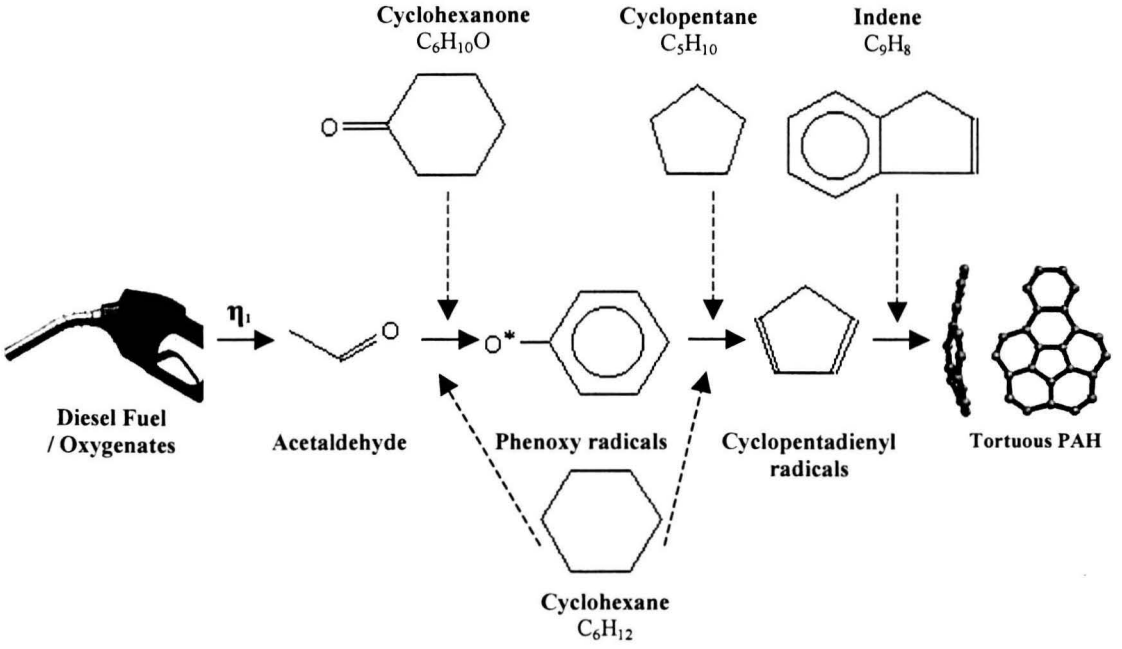

Figure 5.11: Position of the selected fuel additives in the proposed reaction pathway leading to tortuous PAH

Name	Formula	Boiling Point *[K]*	Melting Point *[K]*	Density *[kg/l]*	LHV *[MJ/l]*
Diesel (EN590)	NA	450-650	NA	0.81	36
Cyclohexanone	$C_6H_{10}O$	428	226	0.95	30
Cyclohexane	C_6H_{12}	354	280	0.78	32
Cyclopentane	C_5H_{10}	321	179	0.75	31
Indene	C_9H_8	454	270	0.99	38

Table 5.1: Physical and Chemical properties listed for the selected fuel additives as well as for the reference Diesel fuel

A description of the test engines, emission equipment and test procedures will be presented in the following Chapters.

Chapter 6

Experimental Setup

6.1 Fuel Matrix

All additives selected for investigation in the previous Chapter (table *5.1*) will be blended with low-Sulphur Diesel fuel in a 3:7 ratio or 30 vol-%. Said ratio was chosen because it corresponds to a cyclohexanone/Diesel blend containing 5 wt-% fuel oxygen, allowing for the performance of this oxygenate to be compared to that of two "established" oxygenates (e.g. TPGME and DBM), examined in an earlier study performed at this University [43]. Specifications of the selected base fuel and an overview of the blends in question are listed in table *6.1*.

Blend	Additive	Concentration *[vol-%]*	Density *[kg/l]*	LHV *[MJ/kg]*	Oxygen *[wt%]*
CHO	Cyclohexanone	30	0.85	40.0	5 (nominal))
CHA	Cyclohexane	30	0.81	43.4	0
CPT	Cyclopentane	30	0.79	43.5	0
IND	Indene	30	0.87	42.4	0

Table 6.1: Physical and Chemical properties of the blends under investigation

6.2 Emissions Measurement Equipment

6.2.1 Gaseous Emissions and Smoke Opacity

An extensive description of the methods used to sample smoke opacity and gaseous emissions has been provided elsewhere [43]. Accordingly, a brief overview of the utilized equipment will suffice for this study.

Emission	Range	Working Principle	Device
NO_x	0-10,000 *[ppm]*	Chemiluminescence (CL)	Horiba CLA-720A
HC	0-500 *[ppm]*	Flame Ionization Detector (FID)	Horiba FIA-725
CO	0-2.5 *[vol-%]*	Non-dispersive Infrared (NDIR)	Hartmann&Braun Ukas 3K
Smoke	0-10 *[FSN]*	Filter Smoke Number (FSN)	AVL 415S

Table 6.2: Range and measuring principle of the utilized emission (e.g. gaseous and smoke) measurement equipment

6.2.2 Particulate Mass

When measured, particulate emissions were sampled with a Nova (model: Microtrol) mini-dilution tunnel at a dilution ratio of approximately 10. Sample mass was collected on 70 *[mm]* Pallflex (model: membrane Fiberfilm T60A20) filters, which were equilibrated in a temperature- (295 *[K]*) and humidity- (45 %) controlled environment both prior and post the sampling process. Weighing took place in the same controlled environment on a Sartorius (model: Micro) high precision scale.

6.3 Engine Specifications

The specifications of the two test engines used to ascertain the effectiveness of the aforelisted additives are given in the table below. The stock Euro III DAF engine has been equipped with an EGR system (with CRT[3]) and a VTG[4] in order to comply with the more stringent Euro IV norm. Both engines were fitted with oxidation catalysts.

Engine	**DAF PE235C 4V**	**Volvo DB7**
Bore / Stroke	118 / 140 *[mm]*	104.77 / 130 *[mm]*
No. of Cylinders	6	6
Compression Ratio	16	18
FIE Type	PLD (Pump Line Nozzle)	PLD (Pump Line Nozzle)
Turbocharger	Yes, VTG	Yes, fixed geometry
Charge Cooling	Air-to-water	Air-to-water
EGR	Yes, with CRT soot filter	No
Max. Power	235 kW at 2100 rpm	191 *[kW]* @ 2200 *[RPM]*
Max. Torque	1325 Nm at 1500 rpm	1100 *[Nm]* @ 1300 *[RPM]*
Oxidation Catalyst	Yes	Yes
Emission Norm	Euro III/IV	Euro II
Test Site	Technical University of Eindhoven	TNO / Delft

Table 6.3: Technical data on the two utilized test engines

[3] Continuously Regeneration Trap
[4] Variable Turbo Geometry

Chapter 7

Test Procedures

A total of three engine-related variables will be examined for the their influence on the effectiveness of the blends (table *5.1*) to abate engine-out PM emissions.

- Combustion Phasing
- Exhaust gas Recirculation (EGR)
- Engine Workpoint

7.1 Combustion Phasing

On the DAF engine, the start of combustion can either be advanced or delayed, relative to the crank angle position, by means of altering the start of FIE actuation (SOA[5]). The engine workpoint selected for the SOA sweep is the so-called Road Simulation (ROSI) point (table *7.1*). Operation at this speed and torque mimics a realistic highway situation in Europe (i.e. ~85 *[km/h]*). Note that the corresponding engine settings (table *7.1*) were calibrated to yield a NO_x level of 3 *[g/kWh]*.

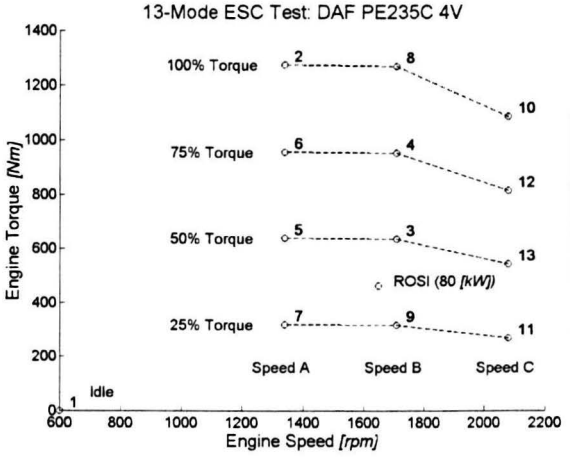

Engine Settings for ROSI Workpoint	
Engine Speed	1650 *[RPM]*
Engine Torque	463 *[Nm]*
Engine Power	80 *[kW]*
Nom. SOA[6]	-13 *[dCa]*
Nom. EGR-Level	15 *[wt-%]*
Charge Pressure	50 *[kPa]*
Charge Temperature	323 *[K]*

Figure 7.1: 13-mode ETC test points as defined for the DAF PE235C 4V Heavy-duty diesel engine.
Table 7.1: Engine settings for the ROSI workpoint

Throughout the duration of the SOA sweep, engine speed/torque, VTG position and EGR-level will be held constant. The SOA will be varied as follows:

$$-13 \rightarrow -8 \rightarrow -13 \rightarrow -18 \rightarrow -13$$

[5] Start of FIE actuation (SOA) → start of fuel delivery (SOD) → start of fuel injection (SOI)
[6] "0 *[dCa]*" corresponds to Top Dead Centre

As the SOA is retarded from –13 to –8 *[dCA]*, more thermal energy will be lost to the environment via the exhaust system. This wasted energy, otherwise converted into (useful) mechanical energy, will manifest in a noticeable decline of fuel economy (figure *7.2*). On the other hand, advancing the start of injection from –13 to –18 *[dCA]* will improve fuel consumption with a comparable factor. Throughout the sweep, however, the A/F-ratio, and therefore the average OCR, is nearly constant (figure *7.3*).

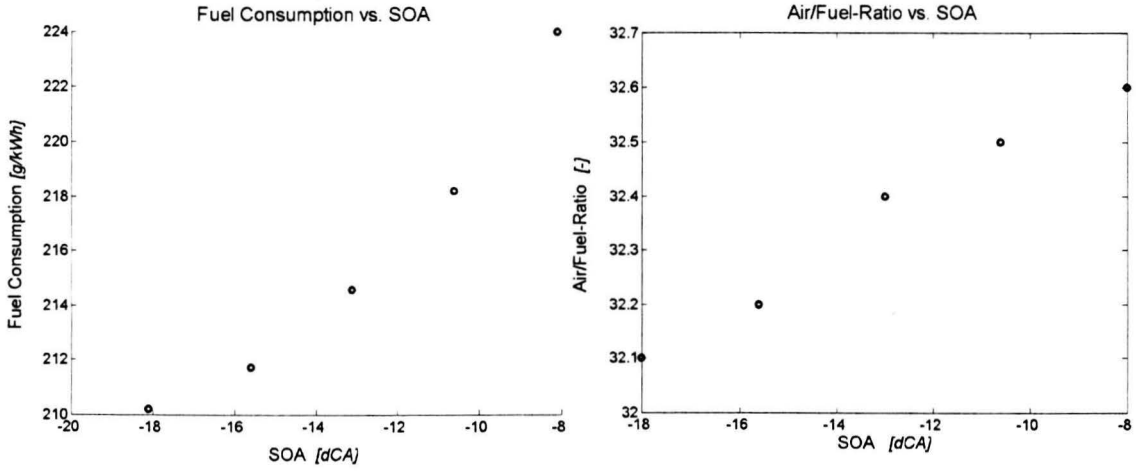

Figure 7.2 and 7.3: Fuel consumption (left) and air/fuel-ratio as a function of the start of FIE actuation (SOA) in the ROSI workpoint. The measurements were performed on the DAF PE235C 4V engine fuelled with EN590 Diesel. Note that "0 [dCA]" corresponds to top dead centre (TDC)

In-cylinder pressure, conversely, which (via the gas law) provides a qualitative indication for the average gas temperature in the combustion chamber, is seen to surge as the SOA is advanced from –8 to –13 [*dCA]* (figure *7.4* and *7.5*).

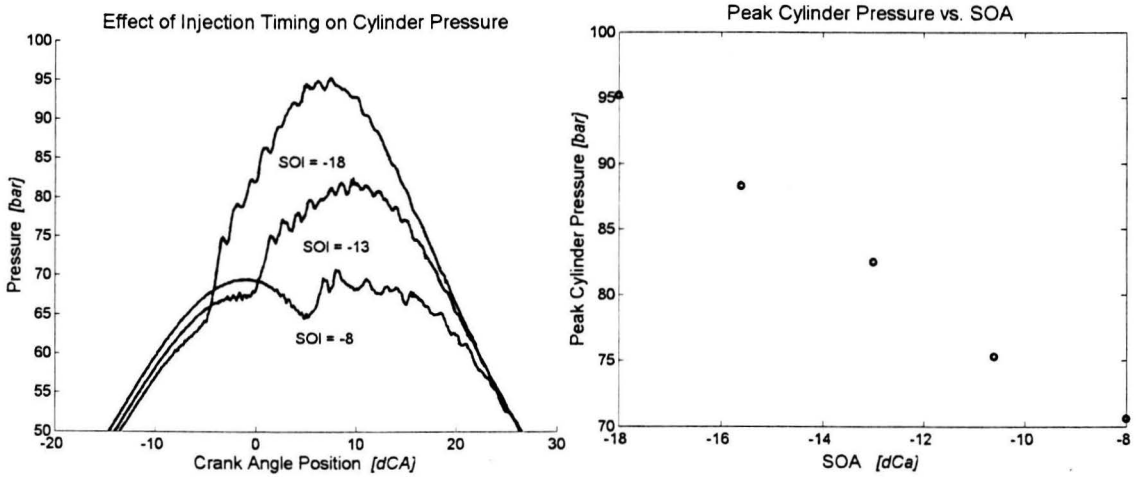

Figure 7.4 and 7.5: Fuel consumption and air/fuel-ratio as a function of the start of FIE actuation (SOA) in the ROSI workpoint. The measurements were performed on the DAF PE235C 4V engine fuelled with EN590 Diesel. Note that "0 [dCA]" corresponds to top dead centre (TDC)

By means of shifting the SOI, one can establish the relevance of in-cylinder temperature/pressure on additive performance, whilst keeping the OCR at a steady level. It will become clear in the following paragraph that a sweep in EGR percentage no longer leaves the OCR untouched. Note that the EGR sweep will be performed on the DAF engine as well.

7.2 Exhaust Gas Recirculation

Altering the quantity of recirculated exhaust gas not only has an effect on the average in-cylinder AFR, but indirectly affects the in-cylinder temperature/pressure as well, via exerting considerable influence on the specific heat of the cylinder charge.

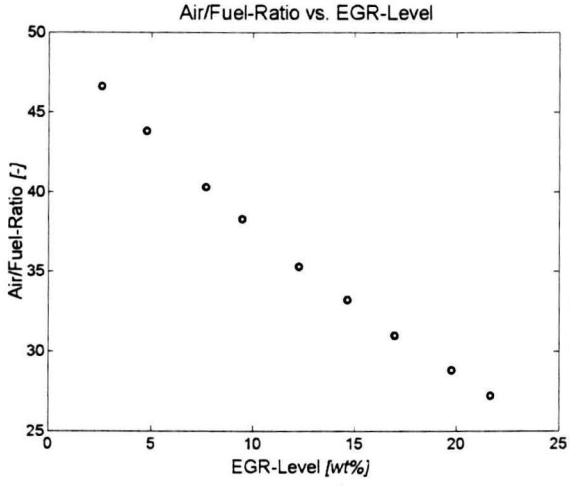

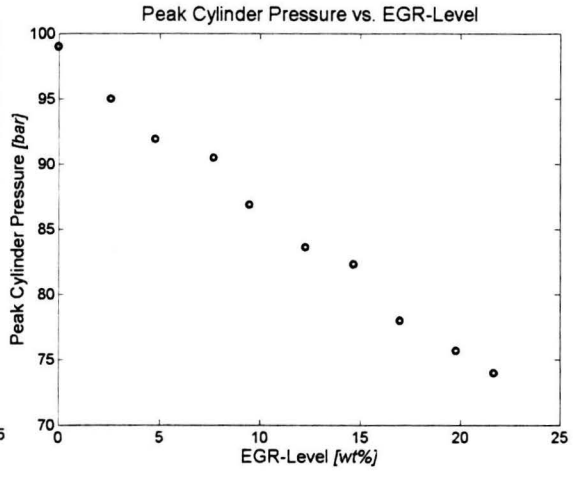

Figure 7.5 and 7.6: Air/fuel-ratio (left) and peak cylinder pressure as a function of EGR-level in the ROSI workpoint. The measurements were performed on the DAF PE235C 4V engine fuelled with EN590 Diesel.

It may be concluded from figures *7.5* and *7.6* that although the EGR sweep results in a spread in peak cylinder-pressure comparable to that observed throughout the SOA sweep (i.e. $\approx$ 30 %), EGR clearly also has a significant impact on the prevailing AFR. Consequently, by means of varying the EGR level (e.g. from 0 to 25 wt-%), one can study the effect of in-cylinder oxygen concentration on the ability of the selected additives to attenuate PM emissions.

7.3 Engine Workpoint

Contrary to the experiments concerning SOA and EGR, the role of engine speed (i.e. reaction time) and torque (i.e. temperature) on additive performance will be investigated on the Volvo engine (table *6.4*). The motivation for a second engine test rig is both practical and scientific in nature.

Considering that the Volvo engine is not equipped with either EGR or the possibility to manipulate the SOA, it cannot be used to determine the impact of these parameters on additive performance. The Volvo test rig, contrary to the DAF one, can be programmed to follow a sequence of workpoints automatically and is therefore the practical choice for examining the influence of engine load and speed on additive performance.

On a scientific note, the choice for experimentation on two test engines allows one to ascertain whether or not additive performance is irrespective of engine technology.

Presented below are the engine workpoints selected for this study, which correspond to the extremities of the 13-mode ESC spectrum (e.g. 2, 7, 10 and 11), as well as a central point (e.g. 3). Because the amount of test fuel was limited, it was decided not to perform a complete ESC test.

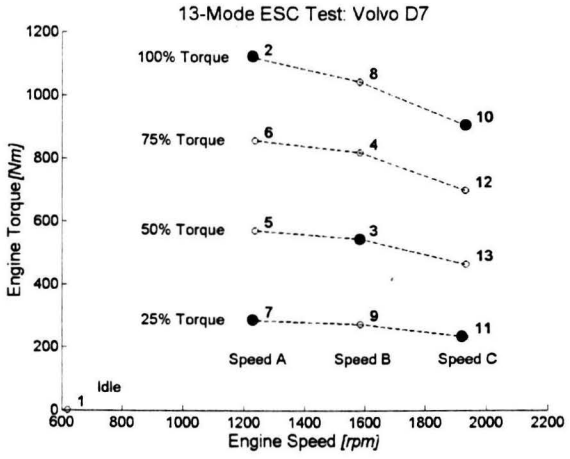

Workpoint	[RPM]	[Nm]
2	1233	1124
3	1585	554
7	1233	296
10	1937	912
11	1936	244

Figure 7.6: 13-mode ESC test points as defined for the Volvo DB7 Heavy-duty diesel engine
Table 7.2: Selected engine workpoint for this study

An third motive for utilizing the Volvo engine, lay in the fact that this set-up includes a mini-dilution tunnel, which is utilized to measure PM mass in all of the selected workpoints. In Appendix D it is shown what the relevance is of measuring both smoke and PM mass simultaneously.

Chapter 8

Analysis of the Results

8.1 *Impact of Combustion Phasing on Additive Performance*

In addition to providing information on the impact of combustion phasing on additive performance, this experiment will also serve as a filter. As this study is limited both by financial and time constraints, only the best performing additive will qualify for further investigation (e.g. impact of EGR and engine workpoint).

Plotted below are the absolute (left) and relative smoke and NO_x values for the various additives blended to 30 vol-% with EN590.

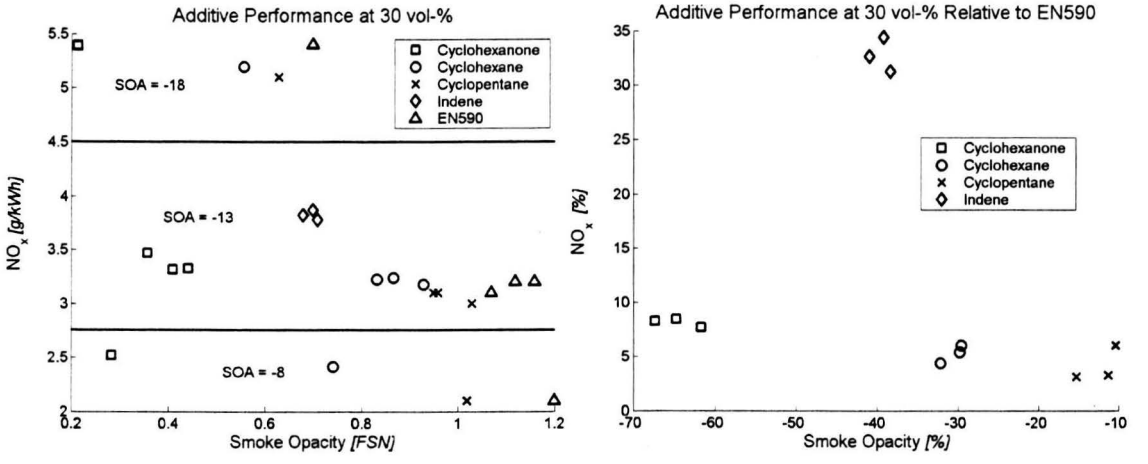

Figure 8.1 and 8.2: Smoke opacity vs. NO_x emissions plotted for all 30 vol-% blends (table 6.1) and base fuel, plotted for various SOA's (left). Reduction in smoke opacity versus the incurred penalty in NO_x in reference to the base fuel plotted for the selected 30 vol-% blends at SOA = -13 [dCa] (right). Data was measured on the DAF PE235C 4V engine in the ROSI workpoint

8.1.1 General Observations

One may deduce from figure *8.1* that with respect to smoke opacity and NO_x all fuels have a shared response to advanced injection timing, namely a decrease in the former and an increase in the latter. Accordingly, in this case, it appears the infamous NO_x / PM trade-off remains intact regardless of fuel composition. Exceptions to the rule are restricted to be the unexpected drop in smoke opacity for the cyclohexanone and cyclohexane blend when the SOI is retarded to –8 from –13 *[dCa]*. Normally, as is the case for the base fuel and the remaining two blends, the lower in-cylinder temperatures intrinsic to retarded combustion phasing, impairs the PM oxidation rate yielding higher PM emissions. It will be made evident in a subsequent paragraph that this peculiar behavior is even more pronounced at elevated additive (e.g. cyclohexanone) concentrations.

Another anomaly is the rather large (~ 40 %) reduction in smoke opacity seen for the indene blend. Generally speaking, an increase in aromatic content results in a (modest) rise in PM emissions.

What is striking as well is the observation that, with the exception of the Indene blend, the penalty in NO_x emissions is rather modest in comparison to the attenuation in smoke opacity (figure *8.2*). Indeed, when comparing cyclohexanone to, for example cyclopentane, there is an enormous dissimilarity in smoke opacity, while NO_x emissions are nearly equivalent. Moreover, judging from the poor NO_x performance of indene, there appears to be no clear correlation between NO_x levels and smoke opacity.

8.1.2 Explanation for the Variation in NO_x Emissions

As can be made clear from figure *8.2*, all additives give rise to a penalty in NO_x emissions. In a fixed engine workpoint, a variation in NO_x amongst fuels is most likely attributable to dissimilar intake pressure and/or ignition quality. The variance in ignition quality can be determined (qualitatively) by comparing the incurred ignition delays (i.e. time period between SOI and SOC). Said delays, in turn, can be read from the corresponding in-cylinder pressure curves (figure *8.3*).

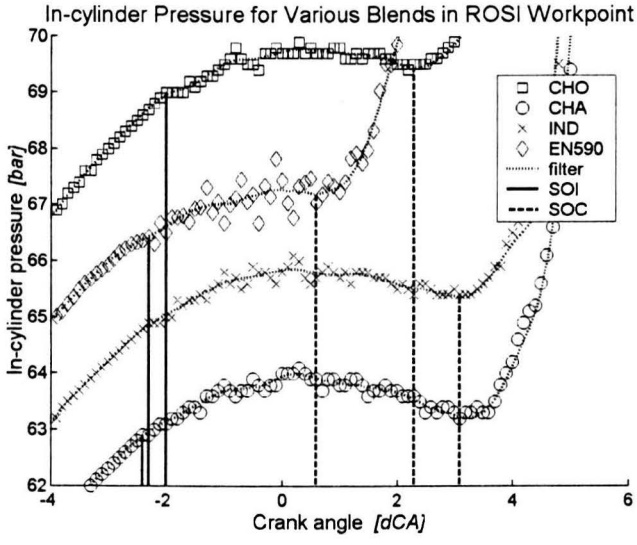

Blend	SOI	SOC	Ign. delay
	[dCA]	*[dCA]*	*[dCA]*
CHO	-2	2.3	4.3
CHA	-2.4	3.1	5.5
IND	-2.3	3.1	5.4
EN590	-2.3	0.6	2.9

Figure 8.3: In-cylinder pressure vs. crank angle position shown here for all additives (save for cyclopentane) at 30 vol-% and the base fuel in the ROSI workpoint (SOA = -13). Data was measured on the DAF PE235C 4V engine. Note that the solid and dashed lines indicate the crank angle position at which the SOI and SOC occur respectively. 0 [dCA] corresponds to TDC

Table 8.1: Approximated values for the start of injection (SOI), start of combustion (SOC), and ignition delay, listed for the cyclohexanone (CHO), cyclohexane (CHA) and indene (IND) blend, as well as for the base fuel (EN590)

Utilizing the lower heating values (table *6.1*), measured injection durations and estimated ignition delays (table *8.1*), one can estimate the amount of (chemical) energy available in the combustion chamber at the time of auto-ignition (table *8.2*).

Blend	Energy consumption	Injection duration	Ignition delay	Available energy at auto-ignition[7]	Intake pressure	EOC pressure
	[kJ/cycle]	*[dCA]*	*[dCA]*	*[kJ]*	*[bar]*	*[bar]*
CHO	2449	9.0	4.3	1170	1.55	70.5
CHA	2536	9.1	5.5	1532	1.435	63.7
IND	2517	8.4	5.4	1618	1.46	66.7
EN590	2570	9.0	2.9	828	1.483	67.4

Table 8.2: Combustion properties of the selected fuels, derived from figure 8.3 and measurements performed on the DAF PE235C 4V engine in the ROSI workpoint. Note that a "cycle" refers to 720 [dCA] (four-stroke engine)

It is evident that all blends have longer ignition delays than the base fuel. As the ignition delay becomes longer, more fuel (i.e. chemical energy) will be present in the combustion chamber at the time of auto-ignition (table *8.2*). Accordingly, one may assume that the fraction of fuel, which is combusted early in the combustion process, increases with the duration of the ignition delay. Peak flame temperature, and therefore NO_x emissions, are naturally affected by this and will generally increase as more fuel is consumed early in the combustion process.

An additional parameter, which affects the (peak) flame temperature, is the prevailing pressure prior to auto-ignition (e.g. end-of-compression (EOC) pressure). As can be deduced from figure *8.3*, there exists considerable spread in this parameter, which can be traced back to the near-linear correlation with intake pressure (table *8.1*). While the combustion process may exert a considerable influence on this parameter via the turbo charger, it is in this case more likely that dissimilar engine settings (e.g. EGR level, VNT position, ambient conditions,..) are to blame for the measured variation in intake pressure.

In order to isolate the effect of ignition delay on (peak) flame temperature, one must therefore compare to fuels, which have similar compression lines (e.g. 30 vol-% indene and EN590). As can be gathered from figure *8.2*, indene yields NO_x levels, which are substantially higher (> 30 %) than those seen for EN590. Accordingly, one may deduce that a longer ignition delay (e.g. 5.4 vs. 2.9 *[dCA]*) manifests higher NO_x emissions.

On the other hand, when one compares two fuels (e.g. CHA and IND) with similar ignition delays (e.g. 5.5 vs. 5.4), but which ignite at different pressures (e.g. ~ 64 vs. ~ 67 *[bar]*), a similar variation in NO_x is observed. Consequently, one may deduce that in-cylinder conditions prior to auto-ignition weigh heavily on the prevailing (peak) flame temperature as well.

It is therefore not surprising that indene, which has both the highest amount of energy available prior to auto-ignition and an average (i.e. compared to the other fuels) EOC pressure, produces significantly more NO_x than for example cyclohexanone (e.g. relatively short ignition delay) and cyclohexane (e.g. relatively low EOC pressure).

[7] Assuming a constant fuel flow throughout the injection process

From a chemical viewpoint, it is interesting to note that as the additive in question has a less reactive[8] molecular structure, the incurred NO_x penalty becomes more pronounced. As discussed at length in Appendix B.1, reactivity (e.g. willingness auto-ignite) is strongly related to the average C-C bond strength. Accordingly, as can be deduced from figure *8.4*, the cetane number, which is a measure for said willingness, of naphthenic molecules (e.g. cyclohexanone, cyclohexane and cyclopentane) is substantially lower than that of n-paraffins, the main constituent of the base fuel. Aromatic molecules, such as indene, are characterized by even more detrimental ignition behavior. All engines parameters being equal, lower cetane numbers tend translate into higher NO_x emissions.

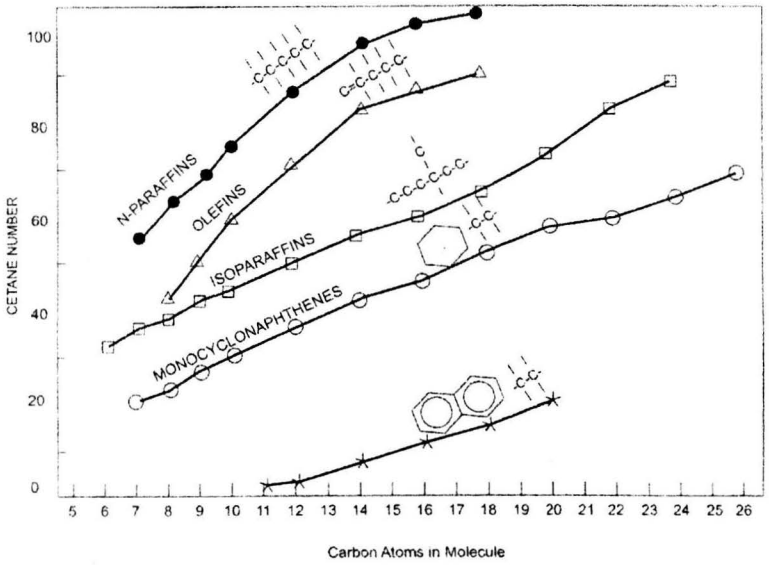

Figure 8.4: Cetane number vs. Carbon number for the various classes of Hydrocarbons [12]

One could therefore attribute the slight increase in NO_x, in the order cyclopentane, cyclohexane, and cyclohexane, to the densities of said additives, i.e. 0.75, 0.78, and 0.95 respectively. Higher densities at equal volume fractions (e.g. 30 vol-%) may be interpreted as more (less reactive) additive molecules per unit of base fuel molecules. Moreover, the particularly poor NO_x performance of indene could have been predicted as well given its relatively high density (~ 1 *[kg/l]*) and its aromatic constituent (figure *8.5*).

8.1.3 Explanation for the Variation in Smoke Opacity

A probable explanation for the variation in PM reducing performance is far less arbitrary. As stated in paragraph 5.5, the additives under investigation were selected based on their (structural) resemblance to probable precursors of tortuous soot (figure *5.11*). With respect to the degree of precursor maturity, one may classify the additives in order: Cyclohexanone → Cyclohexane → Cyclopentane → Indene.

[8] Turn to Appendix D.1 for more information on the reactivity of the various classes of Hydrocarbons

Consequently, based purely on said resemblance, one could have expected a similar order with respect to the reduction in smoke opacity. In reality, however, this order has all but reversed: Cyclopentane → Cyclohexane → Indene → Cyclohexanone. An important conclusion, which must be drawn, is that (unknown) factors, other than structural resemblance to (conjectured) precursors of curved PAH, impact the ability of the selected additives to abate particle emissions. One cannot neglect the fact, however, that all additives brought forth considerable reductions in smoke opacity (figure *8.2*).

Indene

The performance of indene in particular is striking, given the fact that smoke opacity generally tends to increase with fuel aromacity (figure *8.6*). In the figures, below can be seen that while the impact of indene on NO_x emissions is "traditional" (figure *8.5*), its effect on smoke opacity is inconsistent with what one may expect based on the aromatic content of the indene blend (figure *8.6*).

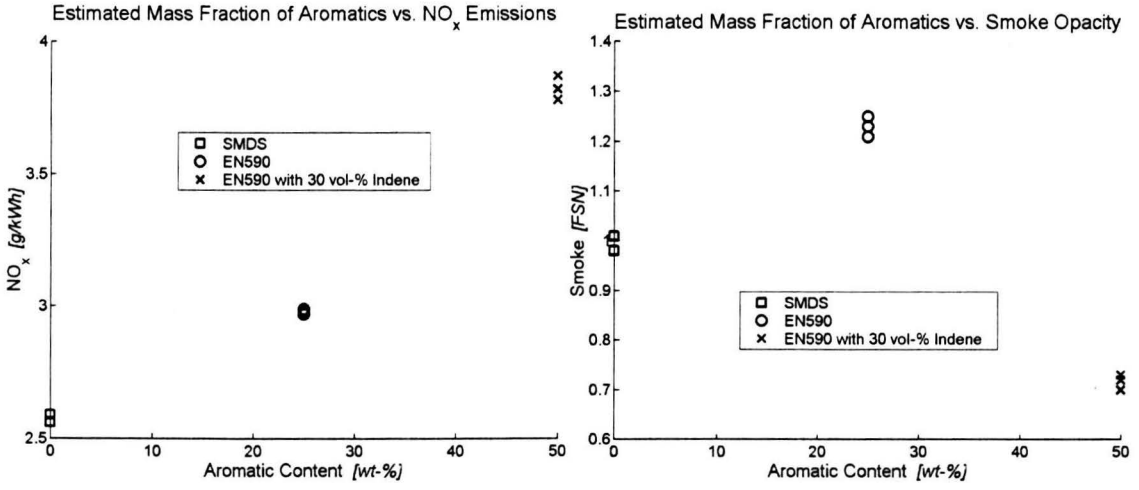

Figure 8.5 and 8.6: NO_x emissions (left) and smoke opacity plotted against the estimated aromatic mass fraction of the fuel. Measurements were performed on the DAF PE235C 4V engine in the ROSI workpoint (SOA –13)

In the opinion of the author, the discrepancy is caused by the addition of a pentagonal ring to the aromatic one (figure *5.11*). Given the inherent presence of indene groups in curved PAH (figure *5.10*), one may assume that these molecules may serve as building blocks for curved PAH. Curved PAH, in turn, as argued in Chapters 4 and 5, yields more readily decomposable particles and ultimately lower PM emissions.

Cyclohexane and Cyclopentane

When comparing the smoke performance of cyclopentane and cyclohexane, it is clear that the hexagonal hydrocarbons outperform their pentagonal counterparts (figure *8.2*). This is an important conclusion, considering the fact that the latter species are essential to the formation of curved PAH.

In the opinion of the author, a possible explanation for this finding may be that the pentagonal chain does not remain intact long enough for it to be incorporated into hexagonal PAH arrays. In a sense, cyclohexane, requiring an extra reaction (e.g. scission) to form a cyclopentane-like molecule, provides for a (chemical) delay. Said delay, in turn, would then allow for these molecules to become available later on in the combustion process. It is stressed, however, that this hypothesis is purely theoretical. The question remains, if not for their resemblance to (potential) precursors of curved PAH, via which mechanism do these cyclic molecules lower the smoke opacity?

Cyclohexanone

Cyclohexanone, previously deemed the underdog of the fuel matrix (paragraph 5.5) actual performed exceptionally well, reducing smoke opacity by more than 60% (figure *8.2*), while increasing NO_x emissions with less than 10 %. Although in the opinion of the author, the strong performance of cyclohexanone should be (primarily) accredited to its conjectured role in the manipulation of particle nanostructure (e.g. promoting curvature), protagonists of oxygenates could make the argument that the low opacity values exist only by the grace of fuel oxygen. When comparing the smoke and NO_x performance of cyclohexanone to that of traditional oxygenates (figure *8.7* and *8.8*), however, one comes across several anomalies.

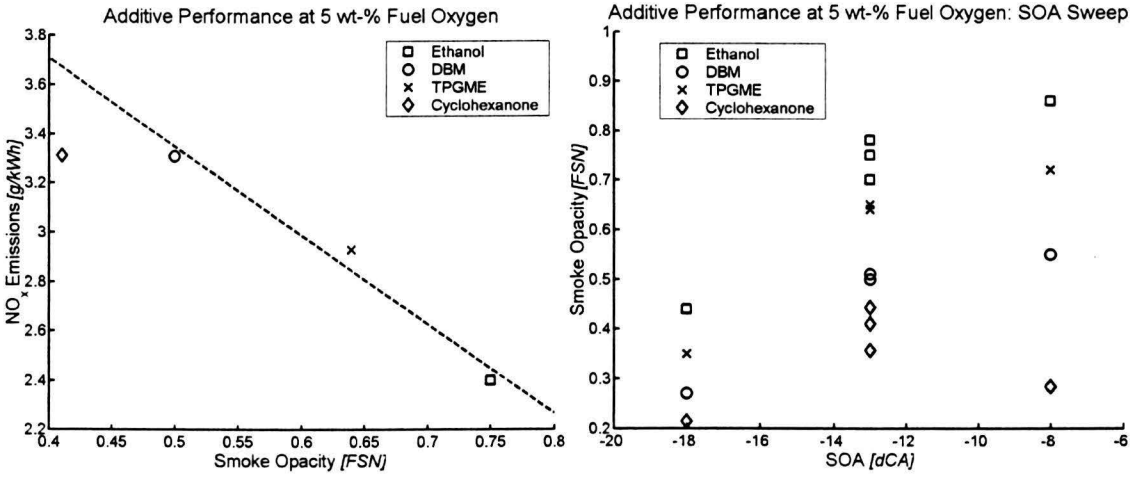

Figure 8.7 and 8.8: NO_x emissions vs. smoke opacity shown for Cyclohexanone and various "traditional" Oxygenates at a SOA of –13 (left). Smoke opacity vs. SOA shown for Cyclohexanone and various "traditional" Oxygenates. Data was measured on the DAF PE235C 4V engine in the ROSI workpoint

First of all, as one may deduce from both figures above, contrary to traditional oxygenates, cyclohexanone does not appear to adhere very well to the NO_x / Smoke tradeoff. Indeed, when retarding the SOA from –13 to –8, cyclohexanone uniquely yields a moderate decline in smoke opacity (figure *8.8*). But also at a fixed SOA of –13 (figure *8.7*), the smoke opacity seen for the cyclohexanone blend appears to be far lower (e.g. ~ 20 %) than one would expect based on the measured NO_x value. Secondly, and perhaps more of importantly, cyclohexanone outperforms the traditional oxygenates regardless of the chosen SOA. Moreover, the relative reduction in smoke opacity seems to augment, as the SOA is retarded from –18 to –8.

As a result of retarding the SOA (e.g. relative increase in combustion chamber volume), the cylinder pressure throughout the combustion process is seen to drop considerably (figure *8.9* and *8.10*). Meanwhile the end-of-compression pressure, conversely, becomes somewhat higher. Said increase, is primarily the result of higher exhaust temperatures, which boost the yield of the turbocharger, thereby raising the intake pressure.

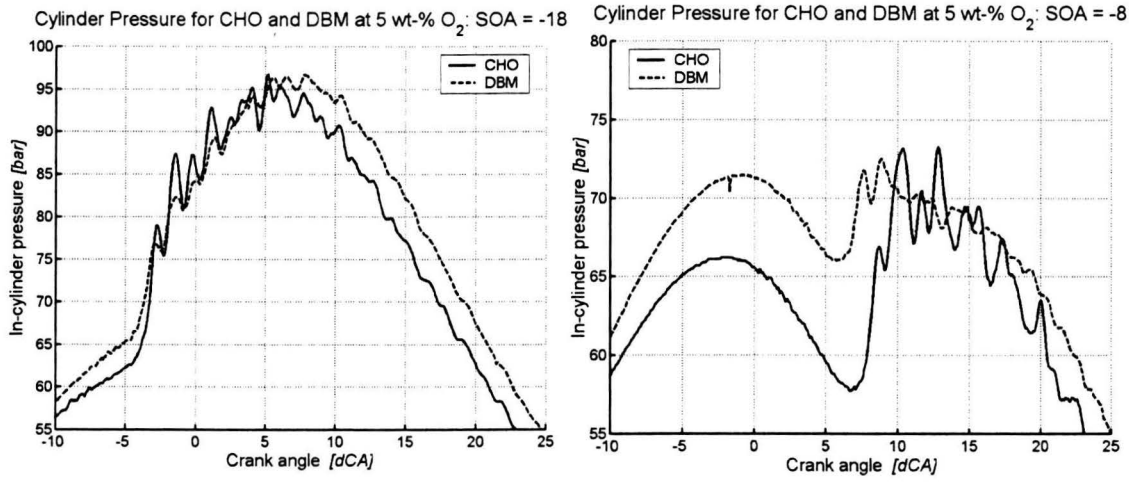

Figure 8.9 and 8.10: In-cylinder pressure vs. crank angle position shown for Cyclohexanone and Dibutyl maleate at SOA = -18 (left) and -8. Data was measured on the DAF PE235C 4V engine in the ROSI workpoint at 15 wt-% EGR

The rate of heat release (ROHR) is affected as well by a shift in SOA. As can be gathered from figure *8.11* and *8.12*, the initial premixed spike becomes considerably higher when the SOA is retarded from –18 to –8. Moreover, the length of the combustion process appears to become shorter.

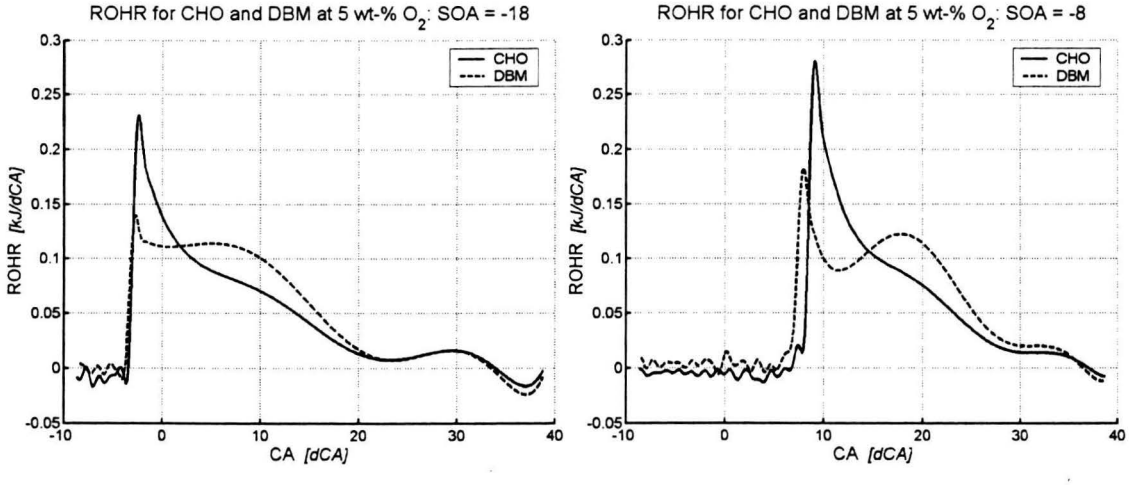

Figure 8.11 and 8.12: Rate of heat release (ROHR) vs. crank angle position shown for Cyclohexanone and Dibutyl maleate at SOA = -18 (left) and -8. Data was measured on the DAF PE235C 4V engine in the ROSI workpoint at 15 wt-% EGR

Seeing as the relative (i.e. to contemporary oxygenates) smoke performance of cyclohexanone is more pronounced at retarded SOA (e.g. –8 vs. –18), one may assume, based on figures *8.9* thru *8.12*, that said performance benefits from a combination of a cooler, shorter combustion and a more dominant initial premixed spike.

If indeed this were to be the case, one would expect the smoke performance to benefit from increasing EGR levels (i.e. lower in-cylinder temperatures) as well. This hypothesis will be subjected to further scrutiny in the following paragraph, which will discuss the effect of exhaust gas recirculation on the performance of cyclohexanone as well as of other oxygenates at equal fuel oxygen levels.

8.2 Impact of EGR on Additive Performance

8.2.1 Air/Fuel-Ratio

As outlined in paragraph 7.2, the concentration of recirculated exhaust gas affects the prevailing OCR. The (negative) effect of EGR on the OCR can be traced back to both a decrease in oxygen and, at high EGR levels (e.g. > 20-25 wt-%), an increase in carbon in the combustion chamber.

Two main causes can be allocated for the aforesaid decrease in oxygen concentration. Considering the fact that exhaust gas is tapped from the exhaust system prior to turbine entry, less energy will be available for air compression when EGR is applied. Intake pressures, therefore, are seen to attenuate with increasing EGR percentage (figure *8.13*). Secondly, EGR implies substitution of oxygen-rich "fresh" air by oxygen-poor exhaust gas. Augmented carbon numbers in the combustion chamber are directly attributable to increased fuel consumption (figure *8.17*).

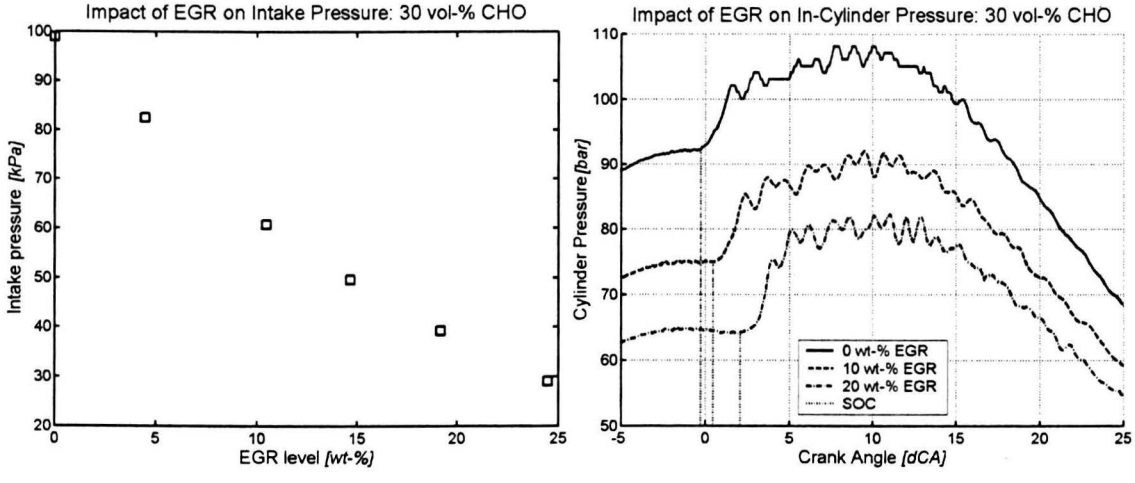

Figure 8.13 and 8.14: Impact of EGR level on intake pressure (left) and on in-cylinder pressure, shown for the 30 vol-% Cyclohexanone blend. The dotted lines indicate the start of combustion. Note that a crank angle of '0' corresponds to TDC. Data was measured on the DAF PE235C 4V engine in the ROSI workpoint (SOA = -13)

8.2.2 Rate of Heat Release

As stated in paragraph 7.2, the working principle of EGR is to suppress in-cylinder temperature by means of raising the in-cylinder concentrations of species with a high specific heat (e.g. H_2O and CO_2). In addition to increasing the specific heat of the "air" supply, application of EGR (in this case) lowers the intake pressure as well (figure *8.13*). It is likely that both factors contributed to the measured decline in EOC pressure seen in figure *8.14*. Based on the Gas Law and the pressure curves plotted in figure *8.14*, one may assume that the EOC temperature will become lower as well, when more EGR is fed into the combustion chamber.

In light of the decline in both EOC temperature and oxygen concentration, it is not surprising that the ignition delay[9] becomes more extended at higher EGR levels (figure *8.14* and *8.15*). Longer delays, in turn, as discussed in paragraph *8.1.2*, allow for a greater fraction of the fuel to be consumed (e.g. release heat) in the initial premixed flame (e.g. spike in figure *8.15*).

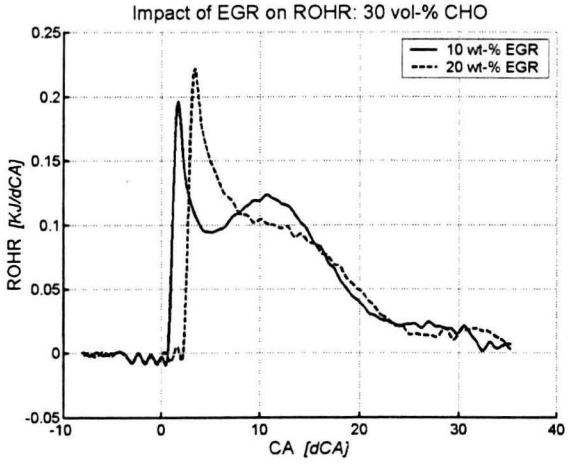

Figure 8.15: Impact of EGR level on rate of heat release, shown for the 30 vol-% Cyclohexanone blend. Note that a crank angle of '0' corresponds to TDC. Data was measured on the DAF PE235C 4V engine in the ROSI workpoint (SOA = -13)

In summation, assuming constant engine operating conditions, one may expect the following three phenomena to occur as one increases the EGR percentage:

- Decline in (average) OCR ↔ decrease in oxygen (figure *8.13*) / increase in carbon (figure *8.16*)
- Decline in end-of-compression pressure ↔ cooler combustion (figure *8.14*)
- Retarded SOC ↔ longer ignition delay (figure *8.14*) ↔ (initial) premixed combustion becomes more dominant (figure *8.15*) ↔ more rapid combustion (figure *8.15*)

[9] Considering the SOA was held constant and one unique fuel was used (e.g. 30 vol-% CHO blend), one may assert that a later SOC corresponds to a longer ignition delay

Note that a cooler combustion and more dominant initial premixed spike were observed (paragraph 8.1.3) as well for CHO and DBM blends (figure *8.9* thru *8.12*) at constant EGR (e.g. 15 wt-%) when the SOA was retarded from –18 to –8. In that case the relative performance of cyclohexanone, with respect to lowering smoke opacity, was considerably higher (figure *8.8*).

8.2.3 Fuel and Energy Consumption

As is true for all oxygen-laden fuels, the (gravimetric) energy density *[MJ/kg]* of cyclohexanone blends is significantly lower than that of regular Diesel fuels. Accordingly, fuel economy *[g/kWh]* worsens as the fraction of cyclohexanone in the blend is raised (figure *8.16*).

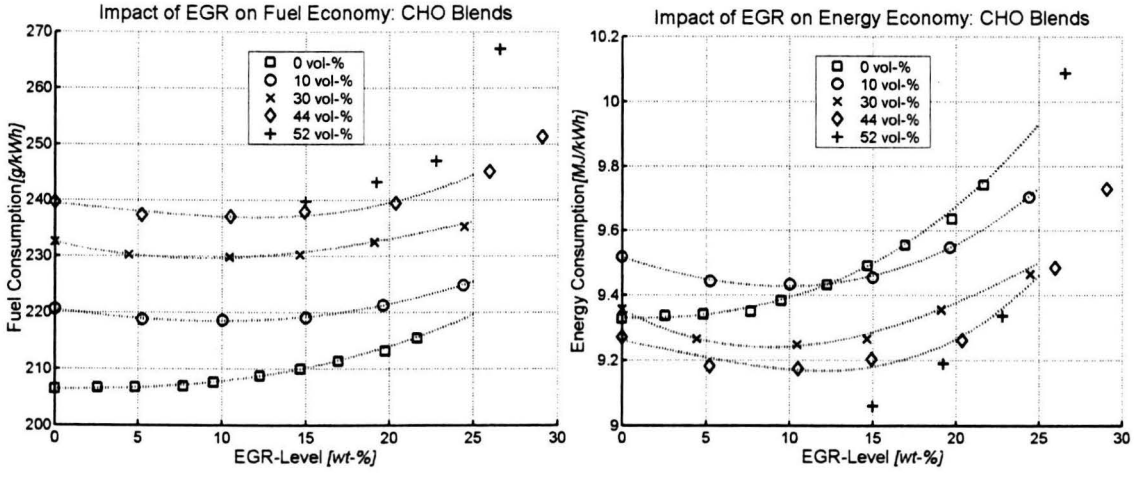

Figure 8.16 and 8.17: Fuel (left) and energy (right) consumption versus EGR-level plotted for various concentrations of Cyclohexanone. Data was measured on the DAF PE235C 4V engine in the ROSI workpoint (SOI = -13)

When considering energy (i.e. *[MJ/kWh]*) rather than mass consumption (i.e. *[g/kWh]*), however, the cyclohexanone blends generally outperformed the base fuel irrespective of EGR level (figure *8.15*). What is more, said distinction became more pronounced as the concentration of cyclohexanone was increased.

It is assumed that the observed increase in thermal efficiency may be traced back to the fact that the combustion process becomes more rapid with increasing CHO concentration (figure *8.18*). Considering more energy (e.g. heat) is released early in the combustion process, this characteristic typically allows for less thermal energy to be lost to the exhaust system.

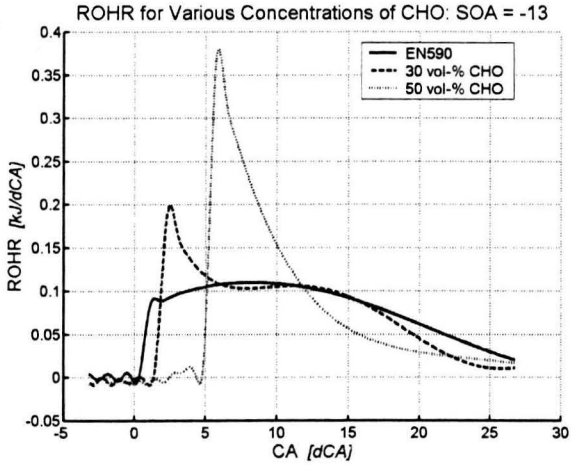

Figure 8.18: Impact of cyclohexanone concentration on the rate of heat release at 15 wt-% EGR. Note that a crank angle of '0' corresponds to TDC. Data was measured on the DAF PE235C 4V engine in the ROSI workpoint (SOA = -13)

One common denominator for all fuels is the rapid increase in fuel/energy consumption seen at high (e.g. > 20-25 wt-%) EGR concentrations (figure *8.16* and *8.17*). It is assumed that at these high EGR levels, oxygen concentrations and in-cylinder temperatures will have fallen to values, which begin to impair flame propagation, ultimately leading to a considerable drop in combustion efficiency (figure *8.19* and *8.20*).

At low-to-moderate EGR concentrations (e.g. < 20 wt-%), however, it is assumed that poorer fuel economy is induced primarily by pumping losses (e.g. in the EGR system).

8.2.3 Unburnt Hydrocarbons and Carbon Monoxide Emissions

Unburnt Hydrocarbons (UHC) and Carbon Monoxide (CO) are the result of a less than ideal (i.e. < 100 %) conversion of fuel molecules into H_2O and CO_2. For Diesel engines operating under normal operating conditions the conversion efficiency is close to 100 %. Consequently, CO and UHC emissions are typically even well below the stringent Euro V norms (figure *8.19* and *8.20*).

Evidently, at EGR levels in excess of ~ 20 wt-%, however, the prevailing low oxygen concentrations and in-cylinder temperature, begin to seriously impair said conversion efficiency (figure *8.19* and *8.20*) regardless of the applied CHO concentration.

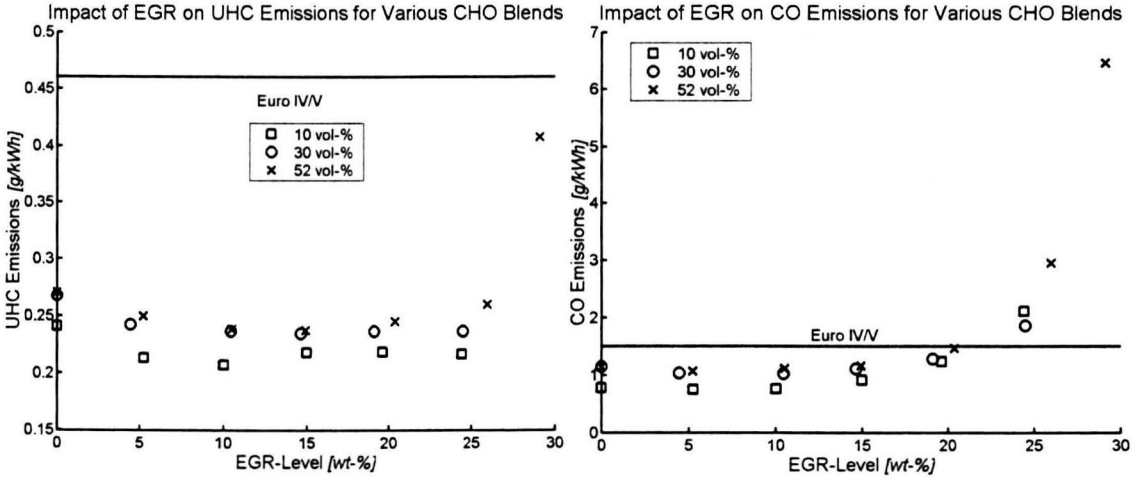

Figure 8.19 and 8.20: Fuel (left) and energy (right) consumption versus EGR-level plotted for various concentrations of Cyclohexanone. Data was measured on the DAF PE235C 4V engine in the ROSI workpoint (SOI = -13). Note that the data plotted in figure 8.19 and 8.20 correspond to the UCH and CO levels upstream of the oxidation catalyst

8.2.4 Smoke Opacity and NO_x Emissions

Plotted in the figure below is the effect of EGR and cyclohexanone concentration on the notorious NO_x / smoke trade-off.

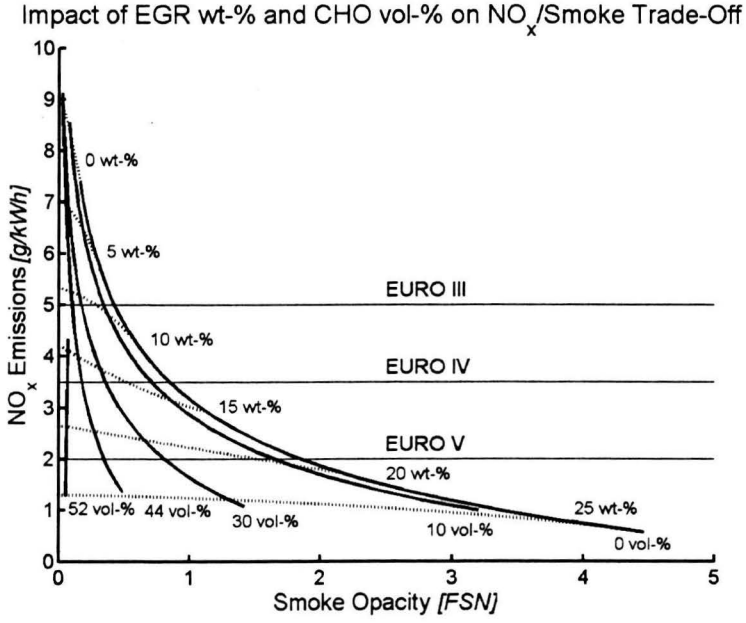

Figure 8.21: Impact of EGR level (dotted lines) and the concentration of cyclohexanone in the fuel (solid lines) on the NO_x / smoke trade-off. Data was measured on the DAF PE235C 4V engine in the ROSI workpoint (SOI = –13)

NO_x

As was previously established for the SOA sweep (paragraph 8.1), the cyclohexanone blend now too consistently yielded higher NO_x levels than the base fuel (e.g. 0 vol-% CHO). Once again one must attribute this increase to the greater reluctance of cyclohexanone to auto-ignite. Said reluctance, in turn, translates into longer ignition delays (figure *8.18*), more rapid combustion (figure *8.18*), and ultimately, higher peak (flame) temperatures (figure *8.3*).

Considering the NO_x formation rate accelerates exponentially with flame temperature, the deterioration of NO_x performance (at constant EGR) with increasing cyclohexanone content (figure *8.21*) is in line with expectations. Irrespective of fuel composition, however, the well-known beneficial effect of EGR on NO_x emissions is clearly visible in figure *8.21*.

Depending on the selected concentration of cyclohexanone, the Euro V NO_x target is reached when the applied EGR level is in excess of ~ 17.5 - 22.5 wt-% (figure *8.21*).

Smoke Opacity

As could be expected, the decline in both in-cylinder temperature and OCR, intrinsic to EGR utilization, manifests in a significant increase in smoke opacity (figure *8.21*). The cyclohexanone blends, however, yield considerably lower opacities than the base fuel irrespective of the chosen EGR percentage. In this, the relative performance augments as the cyclohexanone concentration and/or EGR level is raised (figure *8.21*).

What is more, given ample additive concentrations (e.g. > 50 vol-%), the trend in smoke opacity is seen to remain flat to even slightly negative (figure *8.21*). In other words, utilizing EGR, a 50/50 cyclohexanone/Diesel blend allows for the NO_x emissions to be reduced to the Euro V norm (i.e. 2.0 *[g/kWh]*) whilst maintaining a near zero (e.g. < 0.07) smoke opacity.

The data displayed in figure *8.21* is remarkable to say the least. At the 50 vol-% levels, opacity values are apparently left untouched by attenuating oxygen concentration and lower in-cylinder temperatures. Under said conditions one would normally expect smoke opacity to surge. Indeed, no literature account of similar findings could be found.

One make the argument that either the prolongation of the ignition delay, intrinsic to elevated concentrations of cyclohexanone (figure *8.18*), or the presence of fuel oxygen (e.g. 9 wt-% at 50 vol % CHO), can somehow be held accountable for the preservation of low smoke opacity at high EGR levels.

It has been demonstrated (paragraph 8.1), however, that indene, characterized by even more detrimental ignition quality (i.e. longer ignition delay; table *8.1*), had only half the smoke reducing potential of cyclohexanone at an equal volume percentage (figure *8.2*). Accordingly, one may assert that longer ignition delays alone cannot account for the neutralization of the NO_x / smoke trade-off seen for the 50-vol% cyclohexanone blend (figure *8.21*).

In order to ascertain the relevance of fuel oxygen, the performance of the 50 vol-% cyclohexanone blend, corresponding to 9 wt-% fuel oxygen, will be weighed against that of two established oxygenates at an equal oxygen concentration (e.g. DBM and TPGME).

8.2.5 Cyclohexanone versus Contemporary Oxygenates

It may be deduced from figure *8.22*, that DBM and TPGME, though highly proficient in abating smoke opacity, do not perform nearly so well as cyclohexanone. Indeed, DBM and TPGME (e.g. at 9 wt-% O_2) are outmatched even by the 30-vol% (i.e. 5 wt-% O_2) cyclohexanone blend (figure *8.21*). Accordingly, one cannot attribute the exceptional performance of cyclohexanone to fuel oxygen alone.

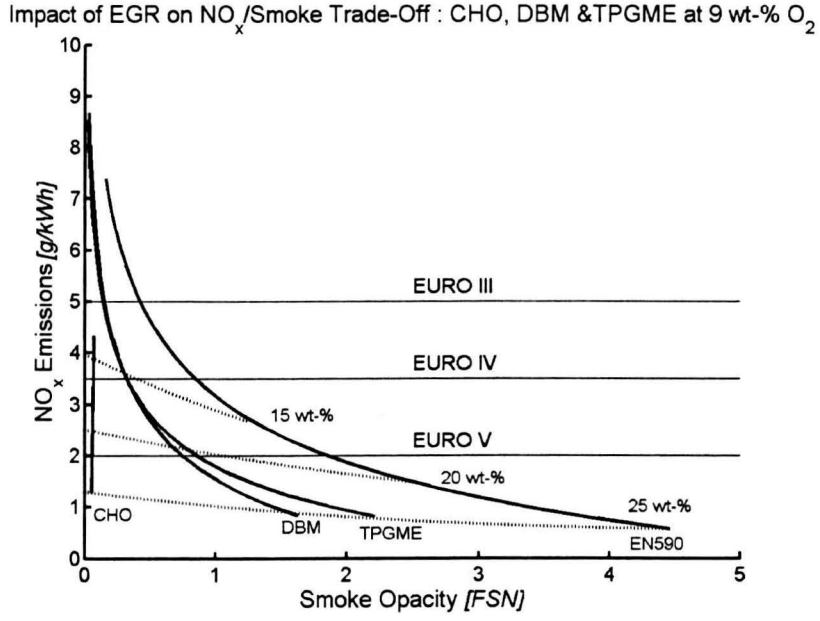

Figure 8.22: Impact of EGR level (dotted lines) on the NO_x / smoke trade-off, plotted for Cyclohexanone (CHO), Dibutyl malaete (DBM), and Tripropylene glycol methyl ether (TPGME) at a constant fuel oxygen content of 9 wt-%. Data was measured on the DAF PE235C 4V engine in the ROSI workpoint (SOI = –13)

Cyclohexanone, despite its unfavorable ignition behavior and therefore relatively high NO_x emissions (figure *8.22*), can still deliver sub Euro V NO_x levels at a far lower smoke opacity (e.g. 0.06 vs. 0.8-0.9 *[FSN]*) than contemporary oxygenates. Now that both fuel oxygen and ignition quality (paragraph 8.2.4) ruled out possible explanations for the astonishing performance of cyclohexanone (figure *8.22*), one must consider a more unorthodox cause. Cyclohexanone was selected specifically for its conjectured proclivity to boost the yield of curved PAH (paragraph 5.5). Accordingly, it is likely that enhanced curvature promotion, rather than fuel oxygen or ignition quality, is responsible for the extraordinary NOx / smoke trade-off (figure *8.22*).

It is of importance, however, to determine whether or not the observed performance of cyclohexanone is unique to either the ROSI workpoint (table *7.1*) and/or the DAF PE235C 4V engine (table *6.3*). To this end, the 30 vol-% cyclohexanone blend, along with TPGME and DBM blends carrying an equal fuel oxygen concentration (e.g. 5 wt-%) will be tested in several other engine workpoints (table *7.2*) on the Volvo DB7 engine rig (table *6.3*).

8.3 Impact of Engine Type and Workpoint on Additive Performance

Depicted below are reductions in smoke opacity, relative to the base fuel, as a function of engine speed (left) and engine torque. Starting with engine speed, one cannot discern any clear correlation with respect to additive performance. At best, one can merely state that the spread in performance in greatest for the cyclohexanone blend. Consequently, one can assume that engine speed does not noticeably influence the smoke reducing capability of either cyclohexanone or the other examined oxygenates. Contrary to what has been proven in the foregoing paragraph, the performance of cyclohexanone is now, on average, no better than that of DBM and TPGME at equal fuel oxygen content. When examining the adjacent graph, however, one comes across a trend, which may prove to be the motivation for said discrepancy.

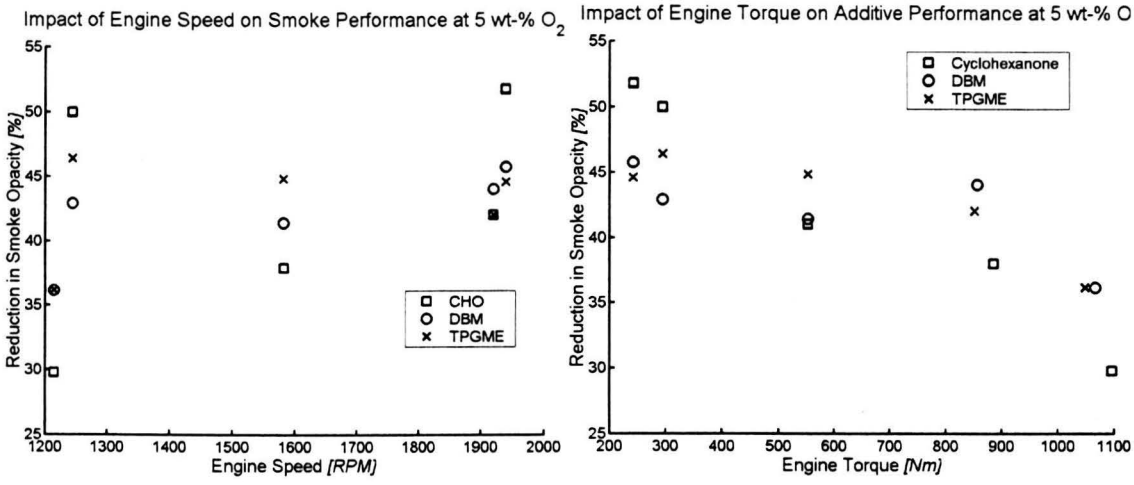

Figure 8.23 and 8.24: Reduction in smoke opacity (i.e. relative to EN590) versus engine speed (left) and torque (right) plotted for various Oxygenates at 5 wt-% fuel Oxygen. Data was measured on the Volvo D7 engine in various engine workpoints (table 7.2)

As mentioned earlier (paragraph 7.3), the Volvo engine, contrary to the DAF engine, is not equipped with an EGR system. As a result, the measured NO_x levels were, in all engine workpoints, considerably higher than those emitted by the DAF in the ROSI workpoint (i.e. 6-8 vs. ~3 *[g/kWh]*). It has been made evident in the previous paragraph (figure *8.21* and *8.22*) that at low EGR levels, corresponding to high NO_x values, the performance of cyclohexanone, with respect to smoke, was no greater than that of DBM or TPGME. A similar correlation with the NO_x level was observed during the SOA sweep as well (paragraph *8.7* and *8.8*).

In both instances, the smoke performance of cyclohexanone relative to other oxygenates is seen to improve as conditions in the combustion chamber become cooler.

A preliminary indication that this phenomenon is not unique to the DAF engine, or ROSI workpoint for that matter, is the fact that the smoke reducing capability of cyclohexanone is seen to deteriorate with augmenting engine load (i.e. in-cylinder temperature; figure *8.24*). Meanwhile, the TPGME and DBM blends appear void of such a correlation.

Conclusion

It has been well established that effectiveness with which cyclohexanone abates smoke opacity has the propensity to increase with lower (mean) in-cylinder temperatures and lower OCR's. Moreover, the method with which the temperature and/or OCR is lowered (e.g. retarded SOA (figure *8.2*), more EGR (figure *8.21*), higher engine load (*8.24*)), does not appear to influence this trend. Cyclohexanone, therefore, behaves fundamentally different than contemporary oxygenates, which clearly do not display so pronounced a thermal dependency (figure *8.1, 8.2, 8.22* and *8.24*).

If one takes into consideration what task cyclohexanone was intended to fulfill, however, it is actually quite logical that this additive performs worse in the presence of higher OCR's and in-cylinder temperatures.

As the reader may recall from Chapter 5, cyclohexanone was selected specifically for its conjectured proclivity to decompose into a pentagonal hydrocarbons, which in turn were believed to promote tortuous PAH, ultimately yielding a more readily combustible particle (nanostructure).

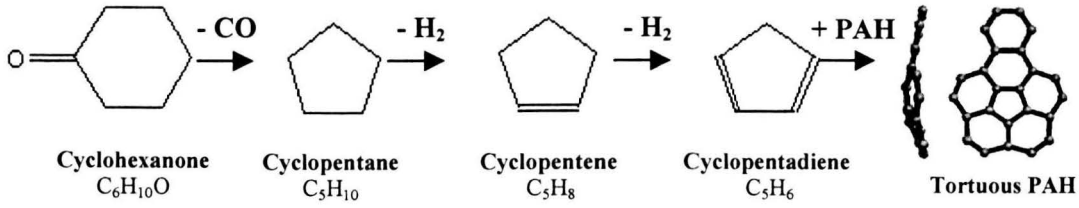

Figure 8.25: Conjectured reaction pathway to tortuous PAH via Cyclohexanone

High oxygen concentrations (i.e. high OCR's) increase the probability of (additional) oxygen atoms bonding to either cyclohexanone or cyclopentane (derivatives), which may cause both the former and latter molecules to decompose into useless (cyclic) C_4-species (figure *5.8*). A similar argument holds for higher in-cylinder temperatures, which not only accelerate the processes described above, but may lead to thermally induced ring rupture as well, yielding various useless (non-cyclic) Hydrocarbons as well. The performance of cyclohexanone, with respect to attenuating smoke opacity, therefore favors a low temperature, oxygen scarce combustion chamber.

The results from this study suggest here that the malevolent effect of low temperatures and oxygen scarcity on the PM oxidation-rate (paragraph 2.6) can be countered by enhancement of particle reactivity (Chapter 3) by way of contaminating its nanostructure with substantial curvature (Chapter 5). As argued in paragraph 2.6.3, the occurrence of pentagonal impurities (figure *8.5*) within the particle nanostructure, allows for particles to decompose even in the absence of oxygen and at a far lower thermal threshold.

Accordingly, given an ample (~ 50 vol-%) concentration, cyclohexanone holds the promise to deliver both the Euro V targets for the gaseous emissions (figure *8.19*, *8.20* and *8.21*) and a smoke opacity (e.g. < 0.07 *[FSN]*), which even by the most conservative estimates (Appendix D), should translate into PM emissions well below the Euro V norm (i.e. < 0.02 *[g/kWh]*). Meanwhile, though penalizing fuel economy *[g/kWh]* due to its relatively low energy density

(figure *8.16*), energy consumption *[MJ/kWh]* for the 50 vol-% cyclohexanone blend is even lower (e.g. > 5 %) than is the case for the base fuel at the EGR percentages requisite (e.g. > 20 wt-%) for Euro V NO_x levels (figures *8.17*).

In any case, the exceptional performance of cyclohexanone, in reference to other oxygenates at an equal oxygen concentration (figure *8.22*), seems to contradict the (unanimous) belief, which is etched deeply in all consulted oxygenate-related literature, namely that fuel oxygen content is (by far) the most dominating factor with respect to oxygenate performance (e.g. PM/smoke). The conjectured subordinance of fuel oxygen to curvature promotion is underlined further by the fact that two non-oxygenated blends (e.g. 30 vol-% cyclohexane and 30 vol-% indene) were found capable of reducing the smoke opacity by more than 30 % and 40 % respectively (figure *8.2*). Said performance nearly matched that of an ethanol blend at 5 wt-% fuel oxygen (figure *8.8*).

Recommendations

Conversion of Smoke Opacity Readings to Particulate Mass Values
As reported in Chapter 7, experiments have been performed on two engine rigs. Only one of which, however, was capable of measuring PM mass directly by means of a mini-dilution tunnel (paragraph 6.2.2). Regrettably, the DAF engine, utilized to ascertain the impact of SOA and EGR on PM emissions, is merely able to measure smoke opacity. PM mass can only be approximated utilizing, among other parameters, the opacity data. The model employed in this work to convert smoke data into PM mass values has been used in the past internally by DAF Trucks NV as well as in an earlier study performed at this University [43].

It was uncertain, however, if this empirical model, though extensively validated on older (i.e. Euro I) engine technology and regular Diesel fuel, is applicable for the more modern engines (i.e. Euro III/IV) and (oxygenated) blends used in this study. To this end, the Volvo data, including both PM mass and smoke data has been used to validate the DAF model. As discussed in depth in Appendix D, the model proved highly inaccurate at smoke opacities relevant for the Euro IV/V PM emission target, predicting as little as 15-20 % of the measured particle mass (figure *D.6*).

Although it was possible to compute a correction factor, with which the error could be limited to acceptable values (formula *D.1*), it is uncertain if this factor is applicable for the DAF engine. It is for this reason that (computed) particle mass values have been omitted from this study, with the only exception being the concluding remark that, that smoke levels less than 0.07 *[FSN]* correspond to sub-Euro IV/V particle emissions.

It is therefore recommended that the 50 vol-% cyclohexanone blend be tested on a modern engine test rig, equipped with both EGR and smoke/particle mass measuring apparati. Furthermore, since measurements on the DAF engine were confined to the ROSI workpoint, it is recommended to test the performance of this blend in all legislated steady-state points (e.g. ESC). Should the performance in other workpoints be on par with that seen in the ROSI point, one could consider performing a complete transient test as well (e.g. ETC).

Compatibility of Cyclohexanone with Elastomers
During operation the DAF engine experienced several cases of elastomer failure. All of which were confined to the fuel injection equipped. In pursuance of the fact that cyclohexanone was not the only fuel examined on this test bed, it is unclear which oxygenate can be held accountable for the degradation of sealants.

It is stressed, however, that said degradation was present only in the DAF fuel injection system, no such failures were recorded on the Volvo engine rig during or after running on cyclohexanone blends.

Prior to more extensive research, however, it is necessary nonetheless to ascertain the elastomer capability of cyclohexanone blends at various concentrations.

Examination of Particle Nanostructure utilizing Trans Electron Microscopy
Throughout this study, it is has been assumed that the measured attenuation in smoke opacity was, at least in part, attributable to the presence of curvature in the particle nanostructure. It would be interesting to test this hypothesis by examining particle nanostructure with the aid of TEM, utilizing techniques similar to those discussed in Vanderwal [6,7], Ishiguro [8] and Su [11,12].

Search for a more Efficient Curvature Promoting Additive
Finally, given the relatively high concentrations of cyclohexanone needed to arrive at the Euro V emission targets, it would of relevance to search for a more efficient additive. In this study, the additives were selected solely on their resemblance of conjectured curvature precursors (figure *5.11*). No doubt, someone more familiar with the reaction kinetics involved in organic chemistry could contemplate a more efficient pathway towards tortuous PAH.

Epilogue

To fight and conquer in all your battles is not supreme excellence; supreme excellence consists in breaking the enemy's resistance without fighting.

- Sun Tzu (544-496 BC) in his work "The Art of War" -

Imagine if you will a terrorist state, the government of which having recently devoted itself to the development of a nuclear weapons program. Once aware of this emerging threat, allied nations confer as to what course of action is most prudent. In pursuance of the fact that the terrorist regime in question has not indicated any willingness to resolve the issue peacefully, a military intervention is considered to be the only viable option.

Preceding the deployment of armed forces, however, the upper echelons of allied governments call for extensive satellite imagery over the area in question. Unfortunately, the obtained data is grounds for serious concern. Apparently weapons-grade Uranium is being smuggled into the country from all points of the compass. On-site intelligence reports disclose that the first of nuclear weapons are nearly operational, requiring only a relatively minute quantity of additional Uranium for completion.

Said terrorist regime, now sentient of allied espionage, cautions that any direct attack on their production facility will be perceived as an act of war. Allied governments, not willing to risk the genesis of nuclear war, concur that interception of the radioactive feedstock prior to entry in the terrorist state is the only way to resolve this delicate situation peacefully. With the clock steadily ticking away, the consensus is to homogeneously disperse as many troops as possible alongside the country's border, effectively forming a blockade.

On a first glance, this would appear to be the logical choice, i.e. attempt to intercept as much Uranium as possible. There are, however, several drawbacks intrinsic to such an approach. In order to ensure as little Uranium as possible reaches the factory, one would have to deploy a considerable number troops in the area. Bearing in mind both the number and scattering of the Uranium traffickers, this tactic is as inefficient as it is costly, not to mention the fact that one could never guarantee the confiscation of all the weapon feedstock in question.

In the aftermath of the nuclear war that followed, the few survivors may have contemplated whether or not the chosen course of action was the right one. In hindsight, perhaps a better approach would have been to somehow sabotage the production process of nuclear weapons. Despite their devastating potential, nuclear warheads are relatively stable, as the fuel (e.g. Uranium) is kept in several subcritical masses in order to avert premature detonation. Once familiar with the inner workings of nuclear bombs, a more cost-effective method of sabotage is readily contrived.

Essentially this approach entails the introduction of slightly modified Uranium into the black market. When this substance, characterized by a considerably smaller critical mass (i.e. less stable), is subjected to both the arduous journey to, as well as the various stages in the weapons factory, premature detonation is now not likely to remain so elusive. Note that the strength of this

technique over the aforementioned blockade approach lay primarily in its low cost and greater effectiveness.

Though any analogy of this narrative with contemporary Diesel technology may seem far-fetched at best, the efforts made by the automotive industry to limit particulate emissions mimic the aforementioned technique of interception. In Diesel engines, said emissions (e.g. nuclear weapons) are generated as a result of local oxygen (e.g. allied troops) deficiencies throughout the combustion phase, which in turn tend to invite the formation of certain particle precursors (e.g. Uranium). In a hitherto successful attempt to abate the concentrations of these essential particle building blocks, the automotive industry has focused primarily on augmenting both the amount of oxygen (e.g. number of troops) and the degree of oxygen distribution (e.g. dispersion of troops) in the flame zone (e.g. weapons factory). Examples for the former and latter approach include turbo charging and higher (fuel) injection pressures respectively.

Unfortunately, both stratagems prove insufficient in meeting the stringent emission legislation set for the near future (e.g. Euro IV/V). To this end, the automotive industry is now investing in two supplementary technologies, i.e. exhaust aftertreatment and fuel modification. The latter of which is currently the most investigated. When applying aftertreatment, which may be regarded as a missile shield in the foregoing analogy, one acknowledges one's inability to attenuate particle emissions to the aspired levels via traditional techniques. Aftertreatment, often materialized in the form of catalysts or filters, is both expensive and intrinsically fuel consuming, and in that trait not a very elegant solution to the dilemma at hand.

With fuel modification, on the other hand, we enter the realm of sabotage. As argued earlier, sabotage is a far less strenuous means towards victory. Two types of fuel additives are currently under investigation at this institute, namely oxygenates and additives designed to manipulate particle nanostructure (e.g. Fullerenization). To the best of knowledge of the author, the latter of which, is virgin territory.

In this, the discrepancy between the two bears reference to the manner in which the particle formation process is sabotaged. With oxygenation, one chemically bonds oxygen atoms to hydrocarbon chains (e.g. ethanol). Given ample fuel oxygen levels, 30-40 % by weight according to the literature, all but a few potential particle precursors are disabled by the presence of a chemically bonded oxygen atom, eventuating in near-zero particle emissions. Fullerenization conversely, involves the doping of fuel with soot-precursor look-a-likes, designed to specifically to self-destruct any ill-fated particle they are incorporated into.

Accordingly, the key discrepancy between these two methods of fuel modification lay in the manner in which the particle formation process is sabotaged. Coming back to the analogy with nuclear warheads, oxygenation may be equated to the modification of Uranium to such a degree of instability that the product will not survive the journey to the weapons factory. With Fullerenization, the instability of the uranium is tailored to the circumstances in the plant, thereby poised to destroy the collective (e.g. warhead) rather than individual components. Assuming for a moment that each warhead (e.g. particle) harbors a number of individual uranium masses (e.g. particle precursors), the strength of Fullerenization over oxygenation, with respect to efficiency, becomes apparent.

Fullerenization, lending its name to the spherical C_{60} Carbon molecule Buckminsterfullerene, may be described as the process of contaminating the predominant soot precursors, poly aromatic hydrocarbons (PAH) (left) with pentagonal impurities (middle). Said endeavor, in turn, manifests in a transformation from a planar to a curved molecular structure (right).

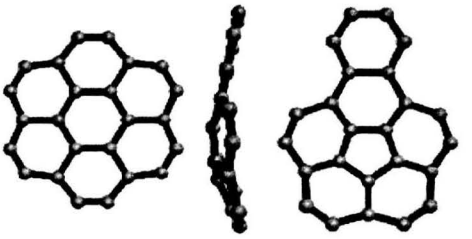

Soot particles, comprised nearly exclusively of groups of stacked PAH, referred to as crystallites, are essentially held together by VanderWaals forces. The strength of this intermolecular force, however, weighs heavily on the spacing between two adjacent PAH. Reaching a minimal value for two perfectly planar PAH, said void would naturally augment with the degree of curvature, eventuating in a rapid attenuation in VanderWaals force. Once exposed to the prevailing flame temperatures, it is assumed that the destabilized soot particle will be more readily combustible than particles containing solely non-curved PAH.

Sun Tzu (544-496 BC), in his work "The Art of War", wrote that *"to fight and conquer in all your battles is not supreme excellence; supreme excellence consists in breaking the enemy's resistance without fighting"*. Arguing that *"All warfare is based on deception"*, Sun Tzu suggests to *"Hold out baits to entice the enemy"*. In essence, the sabotage technique, proposed above is an extrapolation of this 2500-year-old theorem to the modern times. Indeed, interception of uranium (e.g. PAH), necessitating a high degree of "fighting" (e.g. oxygen vs. PAH), is far less elegant a technique than infiltrating sabotaged uranium (e.g. pentagonal impurities) into the weapons factory (e.g. flame zone). "Bait", in this context, is off course the sabotaged uranium (e.g. pentagonal impurities).

References

[1] Dec, J.E., "*A conceptual model of DI diesel combustion based on laser-sheet imaging*", SAE 970873, 1997.

[2] Tao, F. & Chomiak, J., "*Numerical investigation of reaction zone structure and flame liftoff of DI diesel sprays with complex chemistry*", SAE 2002-01-1114, 2002.

[3] Dahlén, L. & Larsson, A., "*CFD studies of combustion and in-cylinder soot trends in a DI diesel engine—Comparison to direct photography studies*", SAE 2000-01-1889, 2001.

[4] Choi, D., Iwamuro, M., Shima, Y., Senda, J. & Fujimoto, H., "*The effect of fuel-vapor concentration on the process of initial combustion and soot formation in a DI diesel engine using LII and LIEF*", SAE 2001-01-1255, 2001.

[5] Flynn, P.F., Durrett, R.P., Hunter, G.L., zur Loye, A.R., Akinyemi, O.C., Dec, J.E. & Westbrook, C.K., "*Diesel combustion: An integrated view combining laser diagnostics, chemical kinetics, and empirical validation*", SAE 1999-01-0509, 1999.

[6] Vander Wal, R.L. & Tomasek, A.J., "*Soot nanostructure: dependence upon synthesis conditions*", Combustion and Flame 136, pp. 129-140, 2004.

[7] Vander Wal, R.L. & Tomasek, A.J., "*Soot oxidation: dependence on initial nanostructure*", Combustion and Flame 134, pp. 1-9, 2003.

[8] Ishiguro, T., Takatori, Y. & Akihama, K., "*Microstructure of diesel soot particles probed by electron microscopy: first observation of inner core and outer shell*", Combustion and Flame108, pp. 231-234, 1997.

[9] Ishiguro, T., Suzuki, N., Fujitani, Y. & Morimoto, H., "*Microstructural changes of diesel soot during oxidation*", Combustion and Flame 85, pp. 1-6, 1991.

[10] Palotas, A.B., Rainey, L.C., Sarofim, A.F., Vander Sande, J.B. & Ciambelli, P., "*Effect of Oxidation on the microstructure of Carbon blacks*", Energy & Fuels 10, pp. 254-259, 1996.

[11] Su, D.S., Jentoft, R.E., Muller, J.O., Rothe, D., Jacob, E., Simpson, C.D., Tomovic, Z., Mullen, K., Messerer, A., Poschl, U., Niessner, R. & Schlogl, R., "*Microstructure and oxidation behavior of Euro IV diesel engine soot: a comparative study with synthetic model soot substances*", Catalysis Today 90, pp. 127-132, 2004.

[12] Su, D.S., Jentoft, R.E., Muller, J.O., Rothe, D., Jacob, E. & Schlogl, R., "*Fullerene-like soot from Euro IV diesel engine: consequences for catalytic automotive pollution control*", Topics in Catalysis 30/31, pp. 241-245, 2004.

[13] Richter, H. & Howard, J.B., *"Formation and Consumption of Single-Ring Aromatic Hydrocarbons and their Precursors in Premixed Acetylene, Ethylene, and Benzene Flames"*, PHYS CHEM CHEM PHYS 4 (11): 2038-2055 2002 .

[14] Frenklach, M. & Wang, H., *"Detailed mechanism and modeling of soot particle formation"*, Soot formation in Combustion (Bockhorn H. (eds.)), Springer-Verlag, Berlin, 1994.

[15] Norton, T.S. & Dryer, F.L., Proc. Combust. Inst. 23, pp. 179-185, 1990.

[16] Kent, P.R.C., Towler, M.D., Needs, R.J. & Rajagopal, G., *"Carbon Clusters near the crossover to Fullerene stability"*, Phys. Rev. B 62, pp. 15394, 2000.

[17] Smith, O.I., *"Fundamentals of soot formation in flames with application to diesel engine particulate emissions"*, Progress in Energy and Combustion Science 7, pp. 275-291, 1981.

[18] Shellswell, R., *"Carbon, its allotropes and structures"*, www.everyscience.com.

[19] Sehar, R. & Lee, K., *"Detailed Technical Data Aids in Diesel Particulate Emissions Control"*, Center for Transportation Research, http://Transtec.anl.gov.

[20] McMurry, J., *"Organic Chemistry, 6th ed."*, Chapter 5, Brook / Cole, 2003.

[21] Yang, Y., Zou, H., Wu, B., Li, Q., Zhang, J., Liu, Z., Guo, X., & Du, Z., *"Enrichment of Large-Diameter Single-Walled Carbon Nanotubes by Oxidative Acid Treatment"*, J. Phys. Chem. B 106, pp. 7160-7162, 2002.

[22] Palotas, A. B., Rainey, L. C., Feldermann, C. J., Sarofim, A. F., & Vander Sande, J. B., *"Soot morphology: An application of image analysis in high-resolution transmission electron microscopy"*, Microsc. Res. Technol., 33, pp. 266– 278, 1996.

[23] Buseck, P.R., Huang, B. & Keller, L.P., *"Electron microscope investigation of the structures of annealed carbons"*, Energy & Fuel, pp. 105-110, 1987.

[24] Lepperhoff, G., *"Influences on the particle size distribution of diesel particulate emissions"*, Topics in Catalysis Vols. 16/17, pp. 249-254, 2001.

[25] Rosner, D.E. & Allendorf, H.D., *"Comparative studies of the attack of pyrolytic and isotropic graphite by atomic and molecular oxygen at high temperatures"*, AIAA Journal, 6, pp. 650-654, 1965.

[26] Lentzner, H., *"Flame lift-off found to affect the evolution of soot in Diesel fuel jets"*, Combustion Research Facility News Vol. 23, No.4, Sandia National Laboratories, 2001.

[27] Cheng, E.A.S, Dibble, R.W. & Buchholz, B.A., *"The effect of oxygenates on diesel engine particulate matter"*, SAE 2002-01-1705, 2002.

[28] Curran, H. J., Fisher, E. M., Glaude, P. -A., Marinov, N. M., Pitz, W. J., Westbrook, C. K., Layton, D. W., Flynn, P. F., Durrett, R. P., zur Loye, A. O., Akinyemi, O. C. & Dryer, F. L., "*Detailed chemical kinetic modelling of diesel combustion with oxygenated fuels*", SAE 2001-01-0653, 2001.

[29] Flynn, P.F., Durrett, R.P., Hunter, G.L., zur Loye, A.O., Akinyemi, O.C., Dec, J.E. & Westbrook, C.K., "*Diesel combustion: An integrated view combining laser diagnostics, chemical kinetics, and empirical validation*", SAE 1999-01-0509, 1999.

[30] Miyamoto, N., Ogawa, H., Nurun, N.M., Obata, K. & Arima, T., "*Smokeless, low NOx, high thermal efficiency, and low noise diesel combustion with oxygenated agents as main fuel*", SAE 980506, 1998.

[31] Hallgren, B.E. & Heywood, J.B., "*Effects of oxygenated fuels on DI diesel combustion and emissions*", SAE 2001-01-0648, 2001.

[32] Shih, L.K.L., "*Comparison of the effects of various fuel additives on the diesel engine emissions*", SAE 982573, 1998.

[33] Vertin, K.D., Ohi, J.M., Naegeli, D.W., Childress, K.H., Hagen, G.P., McCarthy, C.I., Chang, A.S. & Dibble, R.W., "*Methylal and methylal-diesel-blended fuels for use in compression-ignition engines*", SAE 1999-01-1508.

[34] Miyamoto, N., Ogawa, H., Arima, T. & Miyakawa, K., "*Improvement of diesel combustion and emissions with addition of various oxygenated agents to diesel fuels*", SAE 962115, 1996.

[35] Beatrice, C., Bertoli, C., del Giacomo, N. & Lazzaro, M., "*An experimental characterization of the formation of pollutants in DI diesel engine burning oxygenated synthetic fuels*", IMechE C517/023/96, 1996.

[36] Stoner, M. & Litzinger, T., "*Effects of structure and boiling point of oxygenated blending compounds in reducing diesel emissions*", SAE 1999-01-1475, 1999.

[37] Wetsbrook, C.K. & Pitz, W.J., "*Diesel fuel chemistry modelling*", Lawrence Livermore National Laboratory, 2002.

[38] Yeh, L.I., Rickeard, D.J., Duff, J.L.C., Bateman, J.R., Schlosberg, R.H. & Caers, R.G., "*Oxygenates: An evaluation of their effects on diesel emissions*", SAE 2001-01-2019, 2001.

[39] Mueller, C.J. & Martin, G.C., "*Effects of oxygenated compounds on combustion and soot evolution in a DI diesel engine: Broadband natural luminosity imaging*", SAE 2002-01-1631, 2002.

[40] Manuel, A., González, D., Piel, W., Asmus, T., Clark, W., Garbak, J., Liney, E., Natarajan, M., Naegeli, D.W., Yost, D., Frame, E.A. & Wallace, J.P., "*Oxygenates screening for advanced petroleum-based diesel fuels: Part 2. The effect of oxygenate blending compounds on exhaust emissions*", SAE 2001-01-3632, 2001.

[41] Hilden, D.L., Eckstrom, J.C. & Wolf, L.R., "*The emissions performance of oxygenated diesel fuels in a prototype DI diesel engine*", SAE 2001-01-0650, 2001.

[42] Bertola, A. & Boulouchos, K., "*Oxygenated fuels for particulate emissions reduction in heavy-duty DI diesel engines with common-rail fuel injection*", SAE 2000-01-2885, 2000.

[43] Frijters, P.J.M. & Baert, R.S.G., "*Oxygenated fuels for clean heavy-duty diesel engines*", Proceedings of VAFSEP2004, Dublin, Ireland, 2004.

[44] Jones, M., "*Advanced opacity meters: their potential role in future emissions testing legislation for Diesel vehicles*", Proc. of the 6th ETH Conference on Nanoparticle Measurement, Zurich, 2000.

[45] Material Safety Data Sheet (MSDS) for No. 2 Diesel
www.NapaValleyPetroleum.com

[46] Maricq, M.M., Chase, R.E., Podsiadlik, D.H., Siegl, W.O. & Kaiser, E.W., "*The effect of dimethoxy methane additive on diesel vehicle particulate emissions*", SAE 982572.

[47] Liotta, J.F. & Montalvo, D.M., "*The effect of oxygenated fuels on emissions from a modern heavy-duty diesel engine*", SAE 932734.

[48] Kitamura, T., Ito, T., Senda, J. & Fujimoto, H., "*Detailed chemical kinetic modeling of diesel spray combustion with oxygenated fuels*", SAE 2001-01-1262.

[49] Delfort, B., Durand, I., Jaecker-Voirol, A., Lacome, T., Paille, F. & Montagne, X., "*Oxygenated compounds and diesel engine pollutant emissions performances of new generation of products*", SAE 2002-01-2852.

[50] Yoshimoto, Y. & Onodera, M., "*Performance of a diesel engine fueled by rapeseed oil blended with oxygenated organic compounds*", SAE 2002-01-2854.

[51] Akasaka, Y. & Sakurai, Y., "*Effects of oxygenated fuel and cetane improver on exhaust emission from heavy-duty DI diesel engines*", SAE 942023.

[52] Rubino, L. & Thomson, M.J., "*The effect of oxygenated additives on sot precursor formation in a counterflow diffusion flame*", SAE 1999-01-3589.

[53] Spreen, K.B., Ullman, T.L.,& Mason, R.L., "*Effects of cetane number, aromatics, and oxygenates on emissions from a 1994 heavy-duty diesel engine with exhaust catalyst*", SAE 950250.

[54] Tsurutani, K., Takei, Y., Fujimoto, Y., Matsudaira, J. & Kumamoto, M., "*The effects of fuel properties and oxygenates on diesel exhaust emissions*", SAE 952349.

[55] Bertoli, C., del Giacomo, N. & Beatrice, C., "*Diesel combustion improvements by the use of oxygenated synthetic fuels*", SAE 972972.

[56] Uchida, M. & Akasaka, Y., "*A comparison of emissions from clean diesel fuels*", SAE 1999-01-1121.

[57] Nabi, M., Minami, M., Ogawa, H. & Miyamoto, N., "*Ultra low emission and high performance diesel combustion with highly oxygenated fuel*", SAE 2000-01-0231.

[58] Ogawa, H., Nabi, N., Minami, M., Miyamoto, N. & Bong-Seock, K., "*Ultra low emissions and high performance diesel combustion with a combination of high egr, three-way catalyst, and a highly oxygenated fuel, dimethoxy methane (DMM)*", SAE 2000-01-1819.

[59] Kitagawa, H., Murayama, T., Tosaka, S. & Fujiwara, Y., "*The effect of oxygenated fuel additive on the reduction of diesel exhaust particulates*", SAE 2001-01-2020.

[60] Donahue, R.J. & Foster, D.E., "*Effects of oxygen enhancement on the emissions from a DI diesel via manipulation of fuels and combustion chamber gas composition*", SAE 2000-01-0512.

[61] Musculus, M.P., Dec, J.E. & Tree, D.R., "*Effects of fuel parameters and diffusion flame lift-off on soot formation in a heavy-duty DI diesel engine*", SAE 2002-01-0889.

Abbreviations

AFR	=	Air/Fuel Ratio
CHA	=	Cyclopentane
CHO	=	Cyclohexanone
dCA	=	Degree Crank Angle
DBM	=	Di-n-Butyl Maleate
DI	=	Direct injection
ESC	=	European Steady-state Cycle
ETC	=	European Transient Cycle
FIE	=	Fuel Injection Equipment
Glyme	=	Glycol dimethyl ethers
HACA	=	Hydrogen Abstraction and Acetylene Addition
HCR	=	Hydrogen/Carbon Ratio
HDD	=	Heavy-duty Diesel
IND	=	Indene
OCR	=	Oxygen/Carbon Ratio
PAH	=	Poly-Aromatic Hydrocarbons
TEM	=	Transmission Electron Microscopy
TPGME	=	Tripropylene glycol monomethyl ether
SMPS	=	Scanning Mobility Particle Sizer
SOA	=	Start of Actuation
SOD	=	Start of Delivery
SOF	=	Soluble Organic Fraction
SOI	=	Start of Injection

Chemical Formulae

CH_3^-	=	Methyl radical
C_xH_y	=	General formula for Hydrocarbon molecules
$C_xH_yO_z$	=	General formula for Oxygenated Hydrocarbon molecules
CO	=	Carbon monoxide
CO_2	=	Carbon dioxide
H^+	=	proton or Hydrogen atom
O^{2-}	=	Oxygen radical
OH^-	=	Hydroxyl radical
NO_x	=	Oxides of Nitrogen
SO_x	=	Oxides of Sulphur

Symbols

$C_{critical}$	Critical (i.e. for inception) Carbon number	[-]
H/C_{eff}	Effective Hydrogen/Carbon ratio	[-]
Φ	Equivalence ratio	[-]
n	Measure for the size of a PAH array	[-]
T_{flame}	Flame temperature	[K]
x	Number of Carbon atoms per molecule	[-]
y	Number of Hydrogen atoms per molecule	[-]
z	Number of Oxygen atoms per molecule	[-]